Physics – Uspekhi **44** (4) 371 – 396 (2001)

REVIEWS OF TOPICAL PROBLEMS PACS numbers: **07.35.+k**, **62.50.+p**, 91.60.Gf

Shock compression of condensed materials (laboratory studies)

R F Trunin

DOI: 10.1070/PU2001v044n04ABEH000919

Contents

Abstract. Laboratory shock compression data obtained in Russia since 1948 are reviewed, including those for elements and alloys, organic compounds, minerals, rocks, and liquids as well as the hydrides, carbides, and nitrides of metals.

1. Introduction

The A-bomb project in the Soviet Union stimulated the formation and development of a new branch of science, high-density energy physics, which studies the properties of various materials at high pressures and temperatures. Investigations of the properties of shock-compressed materials generalized in the form of their equations of state were primarily applied in the new science to the problem of atomic weapon creation. These equations, which set functional relations between thermodynamic quantities, such as the internal energy (or temperature) of the shock compression, density, and pressure, are necessary to close up the system of equations of fluid dynamics to simulate the construction of nuclear charges and different processes in them.

R F Trunin Russian Federal Nuclear Center, All-Russia Research Institute of Experimental Physics
prosp. Mira 37, 607190 Sarov, Nizhniĭ Novgorod Region, Russian Federation
Tel. (7-831 30) 4-41 18. Fax (7-831 30) 4-59 58
E-mail: root@gdd.vniief.ru

Received 18 December 2000
Uspekhi Fizicheskikh Nauk **171** (4) 387 – 414 (2001)
Translated by K A Postnov; edited by S N Gorin

The relation between the thermodynamic parameters of a shock-compressed material and its kinematic characteristics follows from the mass, momentum, and energy conservation in the algebraic form

$$\frac{V}{V_0} = \frac{D-U}{D}\,, \tag{1.1}$$

$$P = P_0 + \frac{DU}{V_0}\,, \tag{1.2}$$

$$E - E_0 = 0.5(P + P_0)(V_0 - V)\,. \tag{1.3}$$

Here, D and U are the velocities of the shock front and material behind the front (the mass velocity), respectively; P, V, and E are the pressure, specific volume, and internal energy, respectively. The index '0' indicates the initial state of these quantities.

Equation (1.3) determines the so-called Hugoniot adiabat, the adiabat of the material under study, $P_{\rm H} = P_{\rm H}(V, P_0, V_0)$, which is the set of thermodynamic states the material with initial states P_0 and V_0 reaches under shock compression. The shock adiabat is the main source of experimental information underlying the equations of state of various materials. All other shock-wave characteristics, such as the sound velocity behind the shock fronts, the expansion adiabat, and twofold compression adiabat, temperatures of the shocked materials, etc., are directly related to the shock adiabat and determined by its position. This is why the main efforts have been made in studying the shock adiabats, i.e., to find the shock compression curves for different materials.

These studies were initiated in 1948, when the shock compression of uranium was obtained up to a pressure of 50 GPa. Almost simultaneously, compression parameters were measured for uranium and iron up to a huge (at that time) pressure of 500 GPa using a special spherically symmetric device with an accelerating striker (the so-called 'big model' charge, BM) [1]. This value evokes a feeling of respect even nowadays, not speaking of that remote time! Some results were later published in [2].

By 1952, a limiting pressure for heavy metals of 900–1000 GPa was achieved using two-cascade hemispherical charges (TC) [1]. However, there was an uncertainty in the reliability of the parameters obtained due to difficulties in data interpretation, which were caused, in particular, by the necessity to take into account the nonstationarity of the wave process, the substantial heating of the striker, and other factors. At the end of the 1950s, using a slightly modified TC device, a record pressure of 1.8 TPa was attained for shock compression of uranium. The schemes of these charges and the results obtained can be found in [1]. Later on, high reliability and precision of the results were provided by a measuring charge ('soft charge,' SC) [1], which differed from previous setups by using quasi-entropic, heating-free acceleration of the shell-striker and having much more stable characteristics. The SC had significantly fewer shortcomings than previous charges, mainly due to using samples of thickness 3–4 times less than used in BM and TC devices. The SC made it possible to improve earlier results (obtained under pressures of 400–900 GPa) and to substantially broaden the class of materials under study. For example, the list of metals was increased and studies of oxides, hydrides, carbides, and rocks began.

The highest thermodynamic parameters of shock compression were obtained in the middle of the 1990s using the hemispherical SC-18 charge, which had almost limiting characteristics for such devices. The pressure was 2 TPa (2000 GPa) in iron and 2.5 TPa in tantalum.

The maximum pressure for iron, 10 TPa, was obtained in the strong shock of a powerful underground nuclear explosion. The measured compression parameters of materials under such conditions are published in [3] and will not be discussed here. Note that under such huge pressures any material is in the form of a dense ionized plasma with strong interparticle interaction. From this point of view adiabats of any material prove to be similar, which was confirmed in the experiment [3]. Qualitative and quantitative changes along shock adiabats, such as melting, 'solid-state' phase transitions, various electronic transformations, etc., occur at relatively low pressures in the region available for laboratory measurements. Here, we review the results of laboratory studies of the shock compression of a broad class of materials.

2. Methods of study

The shock front velocity D and mass velocity behind the front U are the quantities that can be directly measured in the shock compression experiments. In many cases it is preferable to represent experimental data on the $D-U$ plane rather than in other coordinates. This is partially due to the shock adiabat looking like a linear function on the $D-U$ plane, so that any deviations from linearity are clearly seen in data analysis. This is why many generalizations, in particular the classification of shock adiabats of metals, will be performed using these coordinates. Note that the kinematic parameters (D and U) in the shock compression of materials determine, according to Eqns (1.1)–(1.3), the thermodynamics of the process, i.e., the pressure, specific volume (or density), and internal energy. To find them, no special press equipment, high-precision diamond anvils, etc. are required. It suffices to 'pass' a shock wave through the material under study and measure its kinematic parameters. The shock velocity can be found relatively easily — it is just necessary to set up several transducers of any type sensitive to high front pressures along the shock pathway and to register the wave crossing time between them. As for mass velocities, direct measurements are hampered exactly due to the high front pressures: the transducers must not only 'survive' under such pressures but also register the material velocity behind the shock front. There are some transducers that can be used at relatively low pressures; however, their use under high pressures is limited by many factors, such as their mechanical rigidity in shocks, the electrical conductivity of the material studied, etc.

L B Al'tshuler suggested a quite universal method for mass velocity measurements [4] (the so-called 'braking method'), which is based on sufficiently robust assumptions and can be applied in principle at arbitrarily high pressures. Omitting the details of this method, we point that it involves measurements of the velocity of a plate-striker which is accelerated by expanding products of the explosion. Depending on the type of explosive, the weight of the charge, the construction of the accelerating device, etc., the plate acquires different velocities. When it strikes a 'waiting' target, a shock wave with some intensity appears inside it. The continuity of velocities at the impact boundary implies that for a striker and target made of one and the same material the following equality holds

$$W_{\mathrm{str}} - U_{\mathrm{m}} = U_{\mathrm{m}}\,, \quad \text{or} \quad W_{\mathrm{str}} = 2U_{\mathrm{m}}$$

(here W_{str} is the speed of the striker). In other words, to determine the mass velocity U_{m}, it is necessary to measure the striker's speed at the moment of its impact with the target.

An analysis of the decay of an arbitrary discontinuity at the impact boundary revealed that the method can also be applied for targets made of a different material. In this case an additional condition should be met — the shock adiabat of the striker material should be known. By varying the speed of the striker and measuring D in the target (the material under study) and W_{str}, we determine the location of discrete experimental points on the target's shock adiabat. Using laboratory explosions, the 'braking method' allowed the measurement of shock adiabats of metals over a broad range of pressures from tens of GPa to a maximum value of 2.5 TPa. Under the extreme parameters, the iron striker speed was $W_{\max} = 23$ km s^{-1}. Smaller parameters (up to velocities $W \leqslant 7$ km s^{-1}) are attainable when plane-plate strikers are accelerated in explosion devices in which the explosion produces a plane detonation wave front.

The 'braking method,' being universal and apparently simple, is fairly complicated to realize and is mainly used to determine the shock adiabats of the so-called standard metals. The latter are used as screens through which shocks are transferred into the samples under investigation in the most wide-spread method of shock compression of materials, the method of 'reflection' [4]. This method is also based on the consideration of an arbitrary discontinuity decay, but is 'complicated' by an additional requirement: it is necessary to know the equation of state of the screen material and the

parameters of the shock passing inside it. Let us explain this using the $P-U$ diagram in Fig. 1 as an example. The point of intersection of the wave ray $\rho_{0s}D_sU$ with the adiabat of the screen material determines the initial mass velocity U_1 and pressure P_1 in the screen. The states in the samples studied will be determined by the cross points of their wave rays $0B$ ($0\bar{B}$) with the expansion isentrope P_{ss} of the screen (point *2*) if the material studied is 'softer' than the screen's adiabat, or with the braking adiabat, the twofold compression adiabat (point *3*). To calculate expansion isentropes (or braking adiabats), the equation of state of the screen should be known. However, these calculations are not fully unique since the location of the isentropes (twofold compression adiabats) depends on the chosen (from a usually existing set) equation of state. It is known, however, that for 'small' pressure differences

$$\Delta P = P_1 - P_2 \quad \text{or} \quad \Delta P = P_3 - P_1$$

an isentrope (braking adiabat) approximately coincides with a mirror reflection of the shock adiabat. Quantitative estimates of ΔP in [5], based on the analysis of the mutual location of expansion isentropes calculated for various equations of state, showed that in $P-U$ coordinates at a pressure P_2 equal to 2/3 of the initial pressure P_1, the difference in the location of the expansion isentropes and a mirror 'reflection' from point *1* of the shock adiabat does not exceed 1%, i.e., falls within the experimental error boundaries of the shock adiabat. This allows a more definite setting of measurements, i.e., to choose relations between 'rigidities' of the screen and the material studied. As a consequence, the use of the mirror reflection becomes a simpler and, most important, more definite way of determining the mass velocities in the method of 'reflection.' Most measurements of the compression parameters of matter in shock waves have been made by this method.

The 'braking' method is absolute, since by definition it does not depend on any preliminary conditions. However, with increasing striker velocity its application is complicated by the need to perform heatingless acceleration. This cannot always be done, so in previous systems, in particular in two-cascade charges, the heating of the striker had to be taken into account.

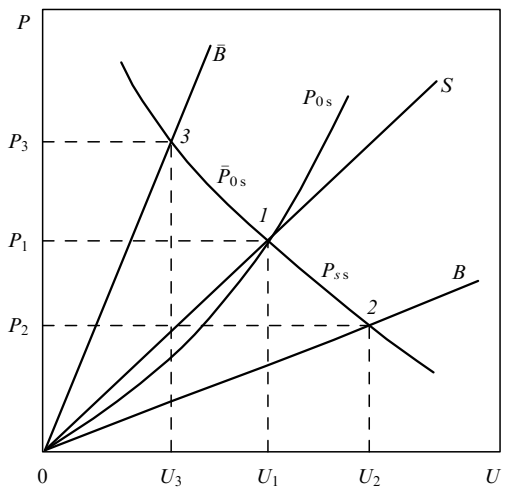

Figure 1. $P-U$ diagram obtained by the reflection method: $0S$ is the wave ray of the screen $P_s = \rho_s D_s U$; P_{0s} is the shock adiabate of the screen; P_{ss} is the isentrope of the screen expansion from the state *1*; and $0\bar{B}$ and $0B$ are the wave rays of the samples studied.

The 'reflection' method is essentially relative: its results depend on the location of the shock adiabat of the screen material, since any change in its location automatically alters the adiabat of the material studied. However, the shock adiabats of standard metals (Al, Fe, Cu), which the screens are made of, determined by the absolute 'braking' method in different laboratories around the world are so steady and stable that one can consider the data obtained by the 'reflection' method equally accurate.

Let us make one more note. We consider shock processes in the so-called hydrodynamic approximation. Strictly speaking, this model can be applied to liquids, i.e., to the states above the shock melting. However, some indirect data [6, 7] indicate that below the melting pressures, a metal behind the shock front is in a relaxed quasi-hydrostatic state. This has been confirmed by results of measurements of the interlayer distance in the shock-compressed molybdenum lattice obtained using the pulse X-ray diffraction analysis [8]. It is logical to explain the results obtained in [8] by the bulk compression of the molybdenum lattice. Finally, the satisfactory agreement between the 'bulk' sound speed (as calculated from the bulk compression modulus) and that derived by extrapolating the shock adiabat to normal conditions (at $U = 0$) at least does not contradict the hydrostatic approximation assumption.

3. Measuring devices

To produce shock waves in the materials with definite and stable characteristics it is necessary to design special measuring devices for as wide as possible a range of pressures. There are two main types of such devices. The first includes 'plane' probes (Fig. 2 a, 2b), in which the following main requirements should be met:

(1) Symmetric flight of the striker; in approaching the target, the deviation from the plane must not exceed 0.1 – 0.3 mm;

(2) Integrity of the plate during the flight, i.e., no cracking, stratification, scabbing;

(3) Stationarity of the shock in the samples during the total registration time;

(4) Stability of shock characteristics of the device ('charge'), in particular, of the striker's speed.

These requirements are met both in plane 'contact' systems [9] (Fig. 2a) and in 'guns' — devices in which an aluminum (with a thickness of 2 – 5 mm in different variants) or iron (steel 3) plate (of thickness 1 – 2.2 mm) accelerated to maximum velocities of 6.5 km s^{-1} [10, 11] (Fig. 2b) is used as a striker. Much higher striker velocities are obtained in spherically symmetric devices [1] (Fig. 2c). In this case, a hemispherical charge of an explosive is surface-initiated by a lens system. The explosion products of an over-compressed detonation wave, by expanding into an air gap, accelerate a steel shell striker. Its velocity gradually increases as it moves towards the center of the system. In modern spherically symmetric probes (such as SCs), the shell velocity varies from $W = 7.2$ km s^{-1} (at 'high' radii) to 23 km s^{-1} at the center of the device. Is it possible to further increase the velocities of the strikers and hence pressures by using explosion devices under laboratory conditions? In principle, the answer should be positive. Indeed, increasing the weight

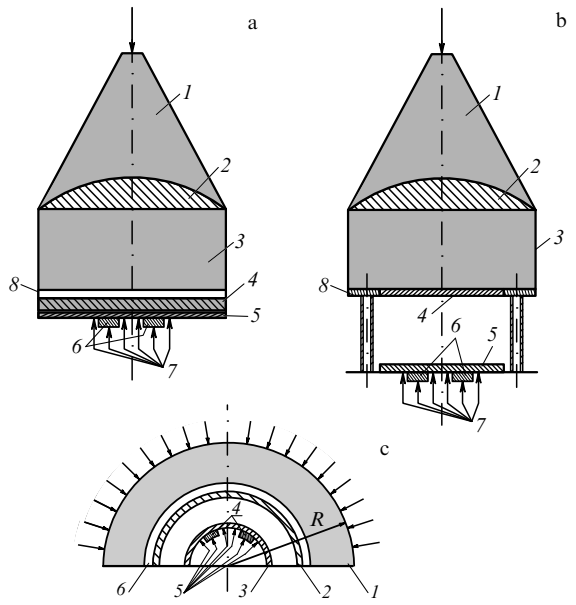

Figure 2. (a) 'Plane (contact)' measuring device: *1*, lens explosive charge transforming the divergent detonation wave into a plane one; *2*, transforming lens; *3*, main explosive charge; *4*, *5*, metal screens; *6*, samples under study; *7*, electrical contact transducers; and *8*, air gap. (b) 'Gun' device: *1–3*, *5–7*, as in Fig. 2a; *4*, striker (Al); *8*, 'supporting' ring (Fe). (c) 'Soft charge' (SC): *1*, hemispherical explosive charge; *2*, shell striker (Fe); *3*, screen; *4*, samples; *5*, electrical contact transducers; and *6*, air gap.

and consecutively the size of charges, using more powerful explosion materials, and some other modifications can increase the limiting parameters of such systems. According to estimates, the real increase can amount to $\sim 20\%$ of the existing values. Clearly, no principally new results can be obtained in this way. At the same time, construction costs of such a huge measuring supersystem will so much exceed the potential gain in results that its development becomes meaningless. Thus, we have reached the limiting possibilities of laboratory systems in getting high pressures with the use of explosives.

Naturally, the accuracy of registration of the compression parameters of the material studied strongly depends on the stability of the characteristics of measuring devices. It is practically impossible to construct ideal devices that reproduce the shock-compression characteristics with the required stability because too many factors affect the final results. But there are some general requirements to minimize the registration errors. They include the stability of physical properties of the explosives (which is achieved by a strict control of the initial components of the mixed explosives), the technology control when manufacturing components and constructing measuring devices, etc.

However, there will be some errors in velocity measurements even provided these requirements are met. To decrease this inaccuracy, each measuring device is used in several (3–6) individual tests with 6–8 independent time registrations within each test. Then the results are averaged. The final error in determination of the wave (and mass) velocities is 1–2 % (depending on the velocity and the number of tests performed with a given measuring device).

As mentioned above, the parameters of the measuring devices can be determined using the 'braking' method in independent tests, so all existing measurement charges (there are about 50 of them) have their own test characteristics of parameters. To register kinematic parameters in our experiments, as a rule we used the electrical contact method, which recorded time intervals on oscillographic or digital registers with an error of ± 5 ns. Some data have been obtained using a photochronographic method of registration.

In the recent papers of Russian and foreign scientists, the shock compression has been measured for a great number of materials, including most elements of the periodic table, many natural and artificial compounds, organic materials, etc. It is not our goal (practically unattainable) to describe all the results of these experiments. Instead, we would like to consider the 'average' adiabat data for the typical representatives of the studied classes of materials, focusing on their peculiarities.

The first materials to have been studied in the laboratory were metals used in the pioneering nuclear charge constructions (uranium, iron, aluminum, etc.). Later on, the need for studies of metal properties became even greater. This was due to an increase of their 'nomenclature' in new constructions of charges and to other reasons, in particular, due to metals being the simplest and at the same time quite varied materials, whose behavior under dynamical action can be studied quite easily and straightforwardly. Thus, we pay most attention to the studies of metals. The results of the shock compression of ordinary metals (in normal initial condition), porous metals (i.e., with decreased initial density) as well as of cooled or melted ones are considered.

In the subsequent sections, the features of the compression of metallic alloys, hydrides, carbides, nitrides, halogenides, oxides, oxygenous salts, minerals, rocks, and organic compounds are discussed. Liquids are studied in the last section; there, we present results of compression measurements of water, water solutions of some salts, and of a large group of organic compounds (alcohols, anhydrides, acids, etc.). The main attention is given to the results obtained by Russian scientists, mainly at the All-Russia Research Institute of Experimental Physics, Russian Federal Nuclear Center, since the majority of such experiments were performed at this institute. For completeness, we cite the results obtained by other scientists.

4. Shock compression of elements

As mentioned above, it is worthwhile systematizing the shock adiabats of elements using their characteristics on the $D-U$ plane. Such an analysis was first suggested in [12]. The experimental data bank significantly increased mostly due to underground nuclear explosion measurements, the expansion of the pressure range available in laboratories (two times for some metals), and new data on the shock compression of nonmetals. This allowed one to improve the classification of the elements [13] using quantitative evaluation of the transition zones between different groups of elements (on the $D-U$ plane). In total, 65 elements of the periodic table have been studied by Russian scientists. The maximum pressures obtained in laboratory reach 1800 GPa for iron, 1000 GPa for aluminum, 2500 GPa for tantalum, and 2100 GPa for molybdenum. More than ten metals have been studied up to a pressure of 1000 GPa, others from 10 (sulfur) to 500 GPa (tungsten).

Before directly considering the shock adiabat classification, we would like to note one common feature: over a wide

range of $D(U)$ dependences, adiabats correspond to linear (or quasi-linear) functions. This well-known behavior has not yet been fully explained. In reality, especially at relatively low velocities, there are some 'perturbations' in the linear relations connected with physical processes occurring during the metal compression, such as reconstruction of lattices, melting, electronic transitions, etc. These processes produce various deviations of the $D(U)$ dependence from linearity, which are the main distinctive features of adiabats of different elements used for their classification. But in general the remarkable property of the linearity of adiabats holds over quite a wide range of kinematic parameters not only for elements, but for other materials as well.

The second note concerns the adiabat slope D'_U. For terapascal pressures ($\geqslant 1000$ GPa), this slope in some models is the same for all elements ($D'_U \approx 1.2-1.3$). Experimentally, at significantly lower compressions, the slope of the adiabats varies from 1.1 up to 1.9 for different metals. Using specific examples, in this review we show not only the tendency of the adiabat slope changes relative to the theoretical values, but in some cases give parameters of the transition zone as well. Figure 3 demonstrates adiabats of Mo and Ta, two representative 'linear' metals. The adiabats of these and six other metals (W, Mg, Na, and apparently K, Nb, and V) are straight lines, and already in the pressure range attainable in laboratories their slopes coincide with the theoretical one. Note that the adiabats of V and Nb can be approximated, as was done in [12], by two crossing lines. However, taking into account the actual experimental accuracy at the maximum shock parameters (hemispherical charges), preference should be given to the single-line linear description [13]. We relate these metals to the first group. The experimental data correspond to a linear approximation over the entire velocity range:

$$D = C_0 + a_1 U\,,$$

where $a_1 = D'_U > 0$, $[U] = \text{km s}^{-1}$.

The slope for V is $a_1 = 1.23$; for Mo, W, Nb, and Mg is $a_1 = 1.25$; for K is 1.17; for Na is 1.27; and for Ta is 1.31. Apparently, some slight changes in the slope cannot be excluded at pressures exceeding 2500 GPa for Ta and 150 GPa for K; however, large changes can hardly be expected.

The second group includes metals that also have a linear $D(U)$ relation, but for which a_1 differs noticeably from the theoretical slope. These metals include the following eight elements:

$$\text{Li}\,(a_1 = 1.07)\,,\quad \text{Be}\,(a_1 = 1.13)\,,$$
$$\text{Re, Ba}\,(a_1 = 1.36)\,,\quad \text{and}\quad \text{Ir, Au, Ca}\,(a_1 = 1.5-1.56)\,,$$

of which two (Li and Be) have $a_1 < 1.25$, so some increase in their adiabat slope is expected. This must take place at higher kinematic parameters than obtained experimentally at present. This change has the 'other sign,' i.e., their adiabat slope must decrease. The adiabats of Li and Ir are also shown in Fig. 3.

The following 15 elements (third type of adiabats) have parabolic $D(U)$ relations and negative coefficients a_2:

$$D = C_0 + a_1 U - a_2 U^2\,.$$

They include

$$\begin{array}{lll} \text{Al}\,(a_1 = 1.36), & \text{Cu}\,(a_1 = 1.50), & \text{Cd}\,(a_1 = 1.76), \\ \text{Pb}\,(a_1 = 1.6), & \text{Cr}\,(a_1 = 1.56), & \text{Ni}\,(a_1 = 1.63), \\ \text{Ag}\,(a_1 = 1.73), & \text{Zn}\,(a_1 = 1.61), & \text{Pd}\,(a_1 = 1.7), \\ \text{Pt}\,(a_1 = 1.56), & \text{In}\,(a_1 = 1.6), & \text{Tl}\,(a_1 = 1.6), \\ \text{Sn}\,(a_1 = 1.69), & \text{Cs}\,(a_1 = 1.58), & \text{Ce}\,(a_1 = 1.94). \end{array}$$

The value of a_2 varies from 6×10^{-2} to 6×10^{-3} km s^{-1}.

All metals demonstrate initial slopes $D'_U > 1.25$, which indicates a decreasing adiabat slope with increasing kinematic parameters. For some metals from this group the transition to the limiting slopes ($a_1 = 1.25$) is already observed in the range of laboratory measurements. This is illustrated by Fig. 4, in which data for copper, cadmium, lead, nickel, and zinc are presented. It is clearly seen how parabolic dependences change to linear ones at high velocities and have similar slopes. Critical wave velocities that characterize the transition to the universal slope $D'_U = 1.2-1.3$ lie in a comparatively narrow range from 10 km s^{-1} (aluminum) to 12 km s^{-1}(iron). (Recall that 'linear' metals, which we referred to the first group, have the limiting slopes over the whole interval of the $D(U)$ relations studied).

What does the equality of the shock adiabat slopes mean? It is logical to admit that this is related to the existence of some general, common characteristics in shocked materials. As the data analysis shows, such a characteristic is the atomic volume of the compressed metals $V_{\text{at}} = A/\rho$. Indeed, at pressures $P > 1-3$ TPa all elements irrespective of their atomic number in the periodic table are characterized by nearly the same $V_{\text{at}} \approx 5 \times 10^3$ nm^3.

Let us turn back to the classification of shock adiabats. A separate small fourth group of elements includes two metals,

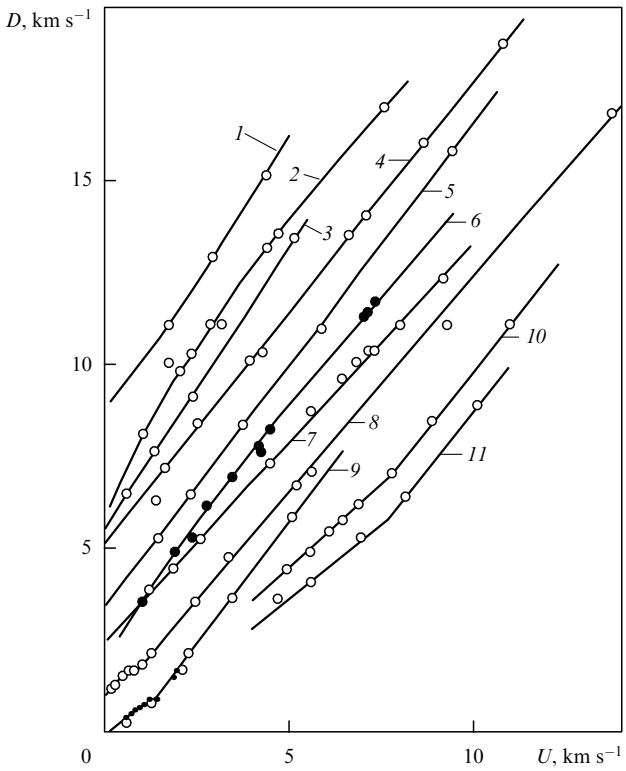

Figure 3. $D-U$ diagrams for metals from different groups (○, ● experimental points): *1*, Co ($D+4$); *2*, Cd ($D+4$); *3*, Ga ($D+3$); *4*, Mo; *5*, Ta; *6*, Pb; *7*, Li ($D-2$); *8*, Ti ($D-4$); *9*, Zr ($D-4$); *10*, Ca ($U-4$); and *11*, Sc ($D-2$, $U-4$)

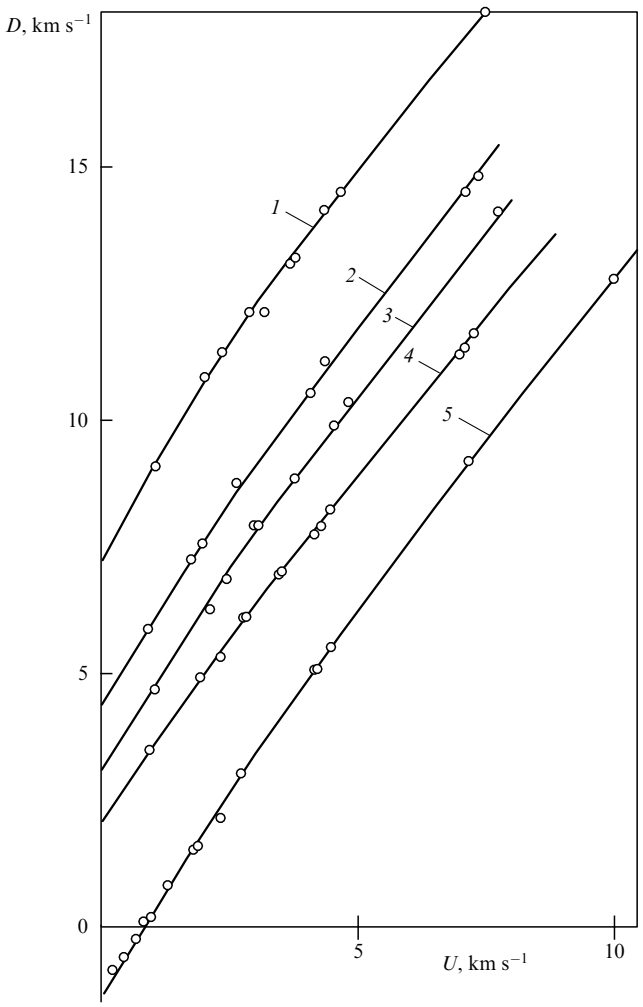

Figure 4. $D-U$ diagram: *1*, Cd ($D+5$); *2*, Ni; *3*, Zn; *4*, Pb; and *5*, Cu ($D-5$).

Co and Rh. They demonstrate parabolic $D(U)$ relations (see Fig. 3), but with a positive coefficient a_2 (a parabola concave downward). While for Rh a linear description with $a_1 = 1.52$ is allowed (the second group of elements), the only description for Co is a parabola with $a_2 > 0$. The reason for such a 'run out' of Co from the general shock-adiabat classification is unclear.

Other elements are characterized by 'nonsmooth' adiabats. The fifth group consists of those elements for which the original structure becomes denser during first-order phase transitions, namely of Fe, Bi, Ti, Sn, Zr, Hf, and Eu. The shock adiabats of these metals (see Fig. 3) have three sections; the first part relates to the initial phase compression, the second (horizontal) one corresponds to a mixture of the initial and high-dense phases, and the third one describes the dense-phase compression. The most famous and well-studied such transition is the $\alpha \to \varepsilon$ transformation in iron. For a number of reasons, including that iron has been sampled as a 'standard' metal, Russian and foreign scientists have devoted special attention to its study.

According to [14], for the α phase of Fe (the first branch, low pressures) we have

$$D = 4.63 + 1.33U\,.$$

For $D = 5.06$ km s^{-1} ($U = 0.322$ km s^{-1}), the $\alpha \to \varepsilon$ transformation begins at a pressure of 12.8 GPa. The transformation ends up at $U_2 = 0.86$ km s^{-1} and $P_2 = 34$ GPa. At higher pressures, dense ε-phase states are realized. Reference [1] lists joint data on the compression of iron obtained using plane and spherical devices and produced by strong shocks in underground explosions. These data can be represented by the following analytical expressions:

$$D = 3.664 + 1.79U - 0.034U^2\,, \quad 1.4 < U < 8\,,$$
$$D = 5.869 + 1.239U + 0.00017U^2\,, \quad 8 < U < 22\,,$$
$$D = 6.982 + 1.190U + 0.00011U^2\,, \quad 22 < U\,,$$

where the velocity U is measured in km s^{-1}. At the conjugate points, the condition of the equality of the wave velocities and their derivatives is met.

The last sixth group includes the following 17 elements: Rb, Ca, Sr, Sc, Y, La, and 11 rare-earth elements from the 6th period of the periodic table. Their characteristic feature is that their adiabats show two parts: a flat one with a slope of $a_1 = 0.7-1.0$ and a steeper one with $a_1 = 1.2-1.7$. The first part corresponds to a linear $D(U)$ dependence. The second part can be equally well fitted by a line or a parabola. Except for Rb from group I of the 5th period of the periodic system, the other five of the elements listed above are located in groups II and III of the 4th and 5th periods. The 6th period includes 11 lanthanides (of 14). Among all the metals that were referred to this group in [12], the data for Rb are the least representative and allow a linear description with $a_1 = 1.27$ within the experimental errors.

It should be noted that the analysis of metals from the sixth group reveals that many of their adiabats cannot be represented by two crossing lines. Distinct breaks are found only for adiabats of Ca, Sc, Y, Lu, Yb, Tu. As for other metals, the shape of their adiabats obtained experimentally can be described both by two crossing lines and a parabola with positive a_2.

From comparison of these two presentations, we deduce that the description of the experimental results by two crossing lines should be preferred. This is caused by the fact that these elements have similar electron-shell structures, the adiabats of some of them display clear breaks, and the $D(U)$ dependences of the others allow such an approximation. The initial flat parts of the adiabats with smaller slopes (see Fig. 3) correspond to strongly compressible states; at the critical (bend) points, adiabats transform to steep lowly compressible parts. Such a configuration of adiabats is determined by the electronic structure of these elements [15, 16], which are characterized by unfilled *s* levels, and by a possible redistribution of electrons under compression, i.e., the transition of the outer *s* electrons to the inner *d* levels. Such a transition is accompanied by a strong compression of the 'empty' *s* shells. As a result, inner closed configurations characterized by a significantly lower compression appear. The change of the flat adiabat branch into a steeper one corresponds to the completion of the transitional processes.

The shock adiabats bends were ascribed in [17] to the shock melting of these metals. However, as shown in [12], such a treatment is not justified and seems to be based on the occasional coincidence of the melting pressure and the pressure at the shock adiabat bends. Moreover, the results of studies of tens of different materials (first of all, elements) demonstrate that the shock-adiabat slopes on the $D-U$ plane practically do not change during solid – liquid transitions.

The changes occur only immediately inside the melting area, but they are usually not detected in the dynamic experiments.

To complete the consideration of the shock adiabats of elements, note the following point: the coefficients C_0 in $D(U)$ relations for $U = 0$ are most frequently close to values of the sound velocities obtained from the isentropic bulk compression moduli $K_{s_0} = \rho_0 C_0'^2$. An analysis [12] of the K_{s_0} determination errors shows that the values of C_0 are essentially within possible determination uncertainties of K_{s_0}. The constant a_1 is expressed through the derivative of the bulk compression modulus at $P = 0$ as

$$a_1 = \frac{1}{4\left[(\mathrm{d}K_s/\mathrm{d}P)_{s_0} + 1\right]} .$$

The constant a_2 can be represented by a more complex relation.

This is the classification of the shock adiabats of elements. It is somewhat arbitrary, because in some cases only limiting experimental data are available, which do not allow the reliable classification of a given adiabat.

In conclusion, we compare the compression of metals from various groups of the periodic system. For example, in Fig. 5 we show dynamic adiabats of metals from three large periods of the periodic system on the pressure – compression ($\sigma = \rho/\rho_0$) plane. First of all, note the difference in compression of alkaline and transition metals. For example, at 100 GPa the compression of potassium (4th period) is about 3.5, while for nickel, which is the transition metal of the same period, $\sigma = 1.3$, i.e., 2.7 times smaller. The compression of cesium is 2.9 times as large as the compression of iridium (for $P = 50$ GPa), both being of the same (6th) period. The reason for this seems to be in the metal structure: we have, on the one hand, 'open' metals with an easily compressed s shell and a single electron weakly coupled with the nucleus, and 'close-packed' transition metals with filled electronic levels on the other hand.

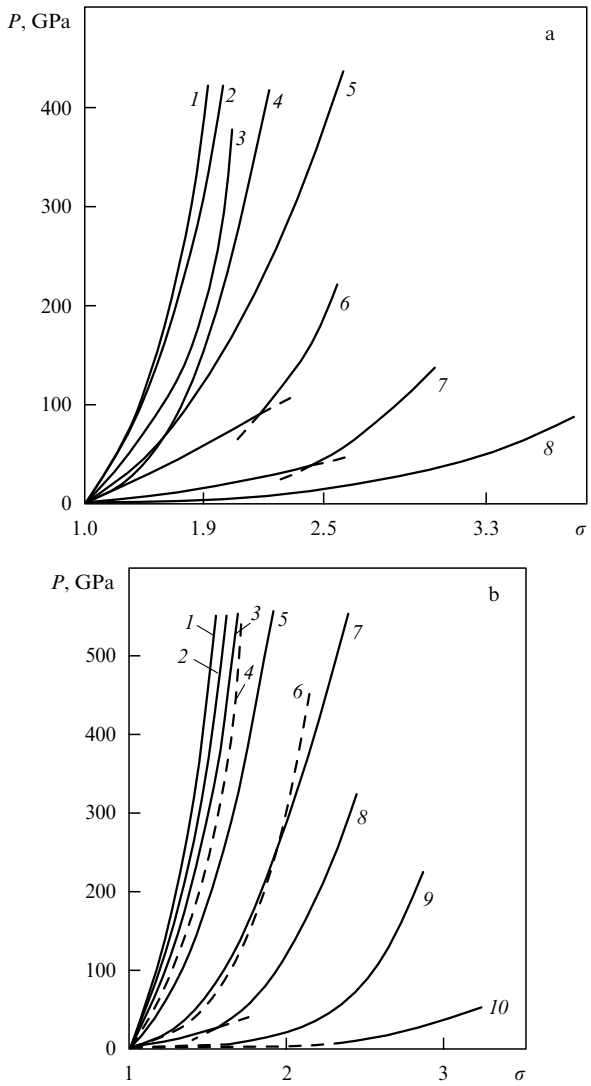

Figure 5. Comparative compressibility of metals from the 4th and 6th periods of the periodic table: (a) *1*, Ni; *2*, Cr; *3*, V; *4*, Zn; *5*, Ti; *6*, Sc; *7*, Ca; and *8*, K. (b) *1*, Ir; *2*, Re; *3*, W; *4*, Au; *5*, Ta; *6*, Tl; *7*, Pb; *8*, La; *9*, Bi; and *10*, Cs.

5. The compression of melted and supercooled metals

So far, we have considered the compression of metals initially at normal temperatures. Below, we present the results of studies of low-melting metals, initially heated to several hundred degrees, where they are in the liquid state.

The goal of the authors of Ref. [18] was to compare the location of the shock adiabats of metals with different initial states: solid and liquid. Probably, in the future it would be possible to change the location of the shock adiabats of metals in the PT diagrams by varying the initial phase states, i.e., to 'control' the phase transitions in materials. Experiments with cooling Bi samples down to $T = -185$°C had the same purposes. The samples studied were heated by a heating wire and cooled by immersing the entire experimental device in liquid nitrogen. The shock compression of Bi, Cd, Pb, Sn, Zn was studied at an initial temperature of +400 °C (liquid state). For Zn, the initial temperature was +450 °C. Data were also obtained for Bi cooled to −185 °C. In Figure 6, we display the results of the experiments in comparison with the 'normal' shock adiabats of these metals ($P = 0$, $T_0 = 20$ °C, $\rho = \rho_0$).

The essential correspondence of the 'hot' and 'normal' adiabats is clearly seen; each of them (for $U = 0$) corresponds to its own bulk sound velocity. Except for Bi, the 'hot' adiabats of metals are located below the 'normal' ones and have a steeper slope D'_U. With increasing shock-wave velocity, the adiabats get closer and near some D_{cr} either merge into one line (Bi, Zn) or the difference between them becomes less than the mutual experimental error. Starting from the same D_{cr}, the slopes of the adiabats converge. This may indicate the 'smoothing' of the metal's phase structure as well, i.e., for the metal melting on the 'normal' adiabat at the corresponding D_{cr}. From this point of view, we carefully analyzed the detailed data on the dynamic measurements of the 'normal' metals from [19]. The experimental data on the shock adiabat of Sn are presented in Fig. 6. A sufficiently complex 'structure' of the 'normal' adiabat of this metal is seen; at $D \approx 4.7$ km s^{-1}, its slope changes repeatedly. The critical wave velocity for tin ($D_{\mathrm{cr}} \approx 4.6$ km s^{-1}) also falls into this velocity interval. It is not excluded that such changes (and coincidences) are due to tin melting on the 'normal' adiabat. The same takes place for three adiabats of Bi. At the point $D_{\mathrm{cr}} \approx 3.5$ km s^{-1}, $U_{\mathrm{cr}} \approx 1.2$ km s^{-1}, all three adiabats have similar parameters and slopes, which also may suggest their identical states. The melting pressures of metals evaluated for the critical parameters D and U are in good agreement with estimates derived from the modern equations of state [20].

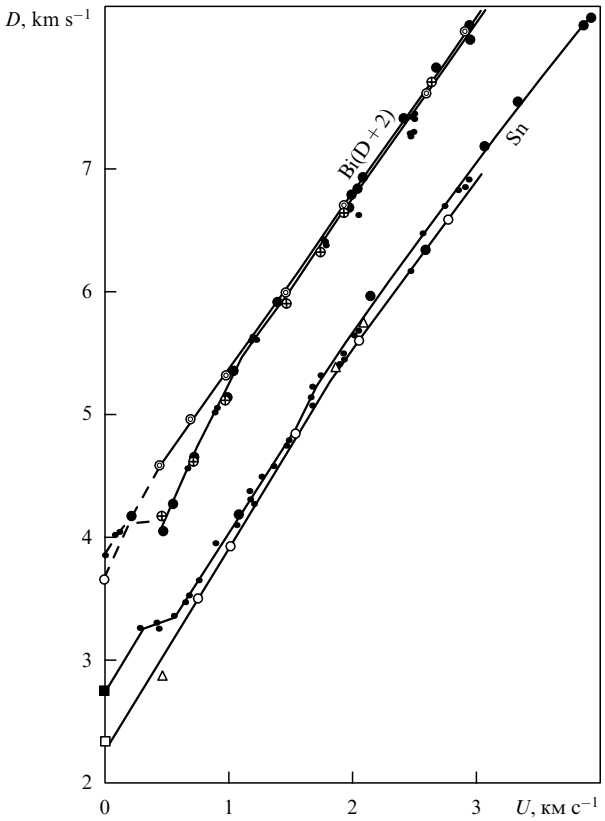

Figure 6. Comparison of 'normal' ($T = 20\,^{\circ}$C, $\rho = \rho_0$) and 'hot' ($T \approx 400\,^{\circ}$C) adiabats (for Bi, the 'cod' adiabat is also shown) (initial temperature of the samples was $180\,^{\circ}$C); ●, •, experimental data for the 'normal' adiabats (•, according to [19]); Δ, ◎, experimental data for the 'hot' adiabats; and ⊕; experimental data for the 'cold' adiabat.

Completing this section, we emphasize that the expressed considerations about shock compression melting are rather qualitative. The final conclusions could be drawn only after the precision and nearly continuous registrations of the kinematic parameters of shock waves.

6. Shock compression of porous metals. Model equations of state

In many cases, for the construction of the equation of state of materials, particularly of metals, the thermodynamic quantities should be known not only near the shock adiabat of the 'solid' material, but also over an essentially broader range of densities and temperatures. The data on the thermodynamics of the high-temperature states come from studies of the shock compression of porous materials, i.e., materials in which in the initial state the individual solid particles with normal density ρ_0 are separated by air (or vacuum) spaces. In this case, the mean density of the porous sample is $\rho_{00} = \rho_0/m$, where m is the degree of porosity. Measuring the shock compression for various m, one can fill considerable part of the $P-\rho$ diagram using adiabats obtained for the solid state ($m = 1$) up to the states with essentially less density (at large m). The effect of density decrease under shock compression is related to thermal processes. Indeed (Fig. 7), at a given pressure $P_{\mathrm{H_1}}$ the thermal energy $E'_{\mathrm{th}} = E_{\mathrm{p}} - E_{\mathrm{c}} = 0.5P_{\mathrm{H_1}}(V_{00} - V_{\mathrm{p}}) - E_{\mathrm{c}}$ of a compressed porous material essentially exceeds the thermal energy of compression of the solid material $E_{\mathrm{th}} = 0.5P_{\mathrm{H_1}}(V_0 - V_1) - E_{\mathrm{c}}$.

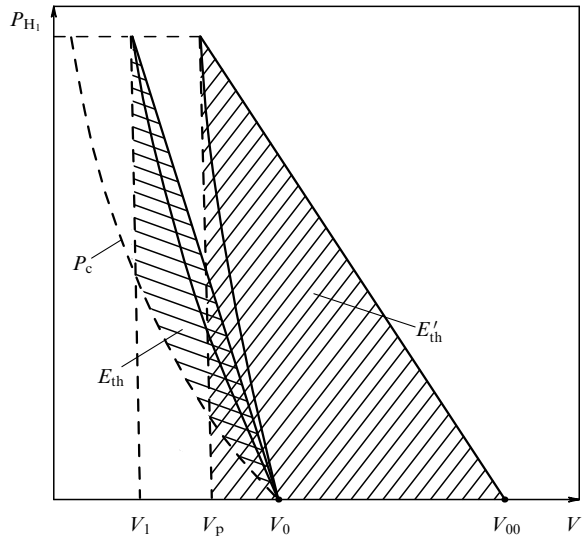

Figure 7. $P-V$ diagram of compression of the 'solid' and 'porous' material.

Here, $V = 1/\rho$ is the specific volume, the index 'c' stands for the 'cold' ($T = 0$ K) compression isotherm. The inequality $E'_{\mathrm{th}} \gg E_{\mathrm{th}}$ (see the hatched regions) also leads to relatively higher temperatures of the porous-material shock compression with respect to the solid one. Naturally, an increase of the porosity leads to a temperature increase (at a fixed pressure). The temperature increase hampers the compression and at some temperature the compressed material density may even not increase but decrease with pressure. The higher V_{00}, the larger (for $P = \mathrm{const}$) is the specific volume of the shock-compressed material (in $P-\rho$ coordinates, the situation is the reverse: the smaller ρ_{00}, the lower the shock compression density).

The first papers in which porous-metal compression was examined in detail were studies of tungsten ($m \leqslant 4$, megabar pressures) [21] and the following four metals: Cu, Al, Ni, and Pb ($m \leqslant 4$, a pressure range two times larger) [22]. Reference [21] was the first to discover the above-mentioned paradox: under high-megabar pressures the density of the compressed porous tungsten had not grown but even decreased! In later Refs [23–25], the porosity of the samples was essentially increased (up to $m = 20$; one experiment for Ni used $m = 28$), the pressure range was enlarged (both to smaller values, down to a few gigapascals, and to larger ones, up to a few terapascals), and the number of materials studied (including metals) was increased.

Before considering the experimental data on porous-material compression, note that, during the studies, dedicated methodical experiments aimed at recovering the possible effects of various factors on the registered parameters of shock waves were performed. To this end, in several series of experiments (done for $m \approx 5-7$) the following quantities were varied:

— the size of the powder particles (from 1 to 100 μm);

— the powder moisture (from the natural value down to zero);

— the sample thickness [from several to tens (~ 80) of mm];

— the presence of air space between the particles.

These factors were shown to insignificantly affect the shock velocity. This allowed the shock-wave regimes realized

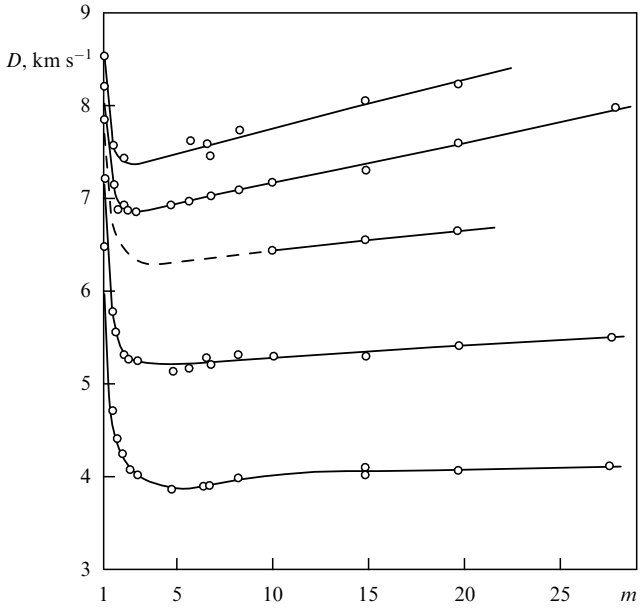

Figure 8. $D-m$ diagram of porous nickel for different shock wave states in the screens.

in these experiments to be considered as being close to equilibrium and thus to reduce the setting of experiments to the standard one (see Fig. 2), and to greatly simplify the experimental data interpretation.

The compression was measured for 15 porous metals: Al, Mg, Mo, Fe, Cu, Cr, Ta, Ni, Pb, Sn, Bi, Co, Ti, W, and Zn. Additionally, porous diamond, graphite, ice, snow, calcite, and silica were studied. Separate measurements were performed for rocks, organic materials, and others. Of metals, the most completely studied was the compression of Ni (14 'porous' adiabats), Cu (9) and Mo (8).

Figure 8 presents data for Ni as an example. These are the so-called 'single charge lines' which illustrate the change of wave velocities as a function of the degree of porosity obtained for equal parameters (for each curve) in the screen of the measuring device. Naturally, other metals demonstrate similar dependences. They share the property of demonstrating a significant change of slopes D'_m (along 'the single charge line'). For small values of wave parameters in the screen and small m, the derivative $\mathrm{d}D/\mathrm{d}m$ was usually negative (a decrease of D with an increase in m). The derivative is $2.0 < m < 3.0$ in the interval $D'_m \approx 0$. For $m > 3$, it either turns positive or remains close to zero (copper, molybdenum). For $m < 2$, the rate of decreasing of $D(m)$ depends on the wave intensity in the screen: the higher the intensity, the smaller the wave-velocity damping in the porous samples. For large enough 'input' parameters, the shock wave velocity can be found constant ($D'_m \approx 0$), and for higher intensities in the screen, the derivative D'_m can become positive. The dependences $D(m)$ allow one to calculate (for known parameters of the shocks in the screens) the location of the shock adiabats for any intermediate m.

Figure 9 summarizes the experimental data on the porous Ni and Cu adiabats on the $D-U$ plane. The experimental points shown in this plot are from papers [11, 19, 23, 25]. The essentially satisfactory agreement between the results is clearly seen.

One of the main features of the plotted adiabats is that the initial parts make up a fan of divergent lines (or low-curved parabolas). This adiabat 'fan' is centered in a small region

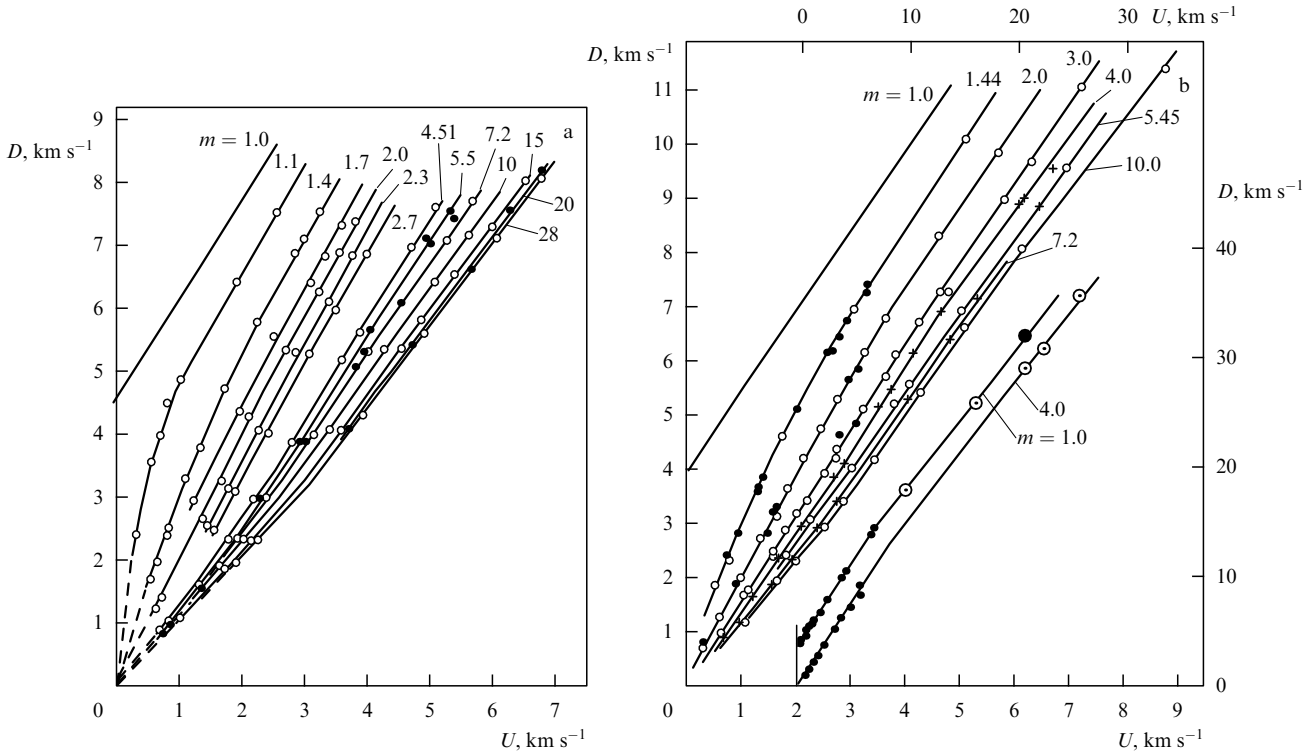

Figure 9. (a) $D-U$ diagrams for (a) nickel and (b) copper. At the bottom of Fig. 9b, laboratory (•) data are compared with the results obtained in the underground nuclear explosions (○ [3], • [26]).

with $0.35 > D_0 > 0.1$ km s^{-1}. It can be assumed that D_0 corresponds to the sound velocity in air reduced by loading the air spaces of the samples by metal particles. Such a treatment should lead to a dependence of D_0 on m: at large m, D_0 is minimal, and vice versa.

The second peculiarity of the adiabats is associated with the alignment of their slopes. While on the initial part the slopes D'_U are strongly different (the largest slopes are observed at small m), they gradually converge with increasing velocities approaching the slope of the 'solid' ($m = 1$) adiabat. Similar to the latter, for high shock velocities the slopes of the porous-metal adiabats tend to $D'_U = 1.25$, in accordance with the value predicted from theoretical models of the compressed material at ultrahigh pressures. This is illustrated by Fig. 9b. At the bottom, data for Cu are shown that were obtained from underground nuclear explosions with the maximal shock wave parameters.

Finally, note one more important fact, that the shock adiabat for nickel with a porosity of $m = 28$ ($\rho_{00} = 0.315$ g cm^{-3}) is located immediately close to the boundary line $D = D_0 + U$ parallel to the bisector $D = U$. At $D \approx 3.4$ km s^{-1}, the difference in U between these lines does not exceed 0.05 km s^{-1}! This indicates that adiabats of all the porous metals with $m > 30$ are literally nearly stuffed into that interval of mass velocities! Since the accuracy of U determination for these parameters is comparable with the interval itself, the further advance into the $m > 28$ region becomes little justified. To evaluate the location of shock adiabats for such a high m it is sufficient to use the available adiabat of the porous nickel with $m = 28$ (with some correction, perhaps).

Let us consider now $P-\rho$ diagrams for metals. In Figure 10, we plotted data for nickel, the most completely studied metal. Obviously, shock adiabats spread over a significant part of the diagram. Each of them is characterized by two parts: the first, flat, and the second, steep. The slope on the second part depends on m. For small m ($m < 2$), we have $\partial P/\partial\rho > 0$; for $m \approx 2-3$, the adiabats are close to verticals; for $m > 5$, they correspond to either negative or sign-alternating derivatives. This situation is due to a strong change in the thermal properties of the metal, in particular the change of the Grüneisen coefficient $\gamma(E, V) = V(\partial P/\partial E)_V$ from values typical for solid state ($\gamma > 1$, as a rule) up to the limiting parameters corresponding to a highly heated gas ($\gamma \approx 2/3$).

As shown in [22], changes in the slopes of porous-metal adiabats in different regions of the $P-\rho$ diagram directly

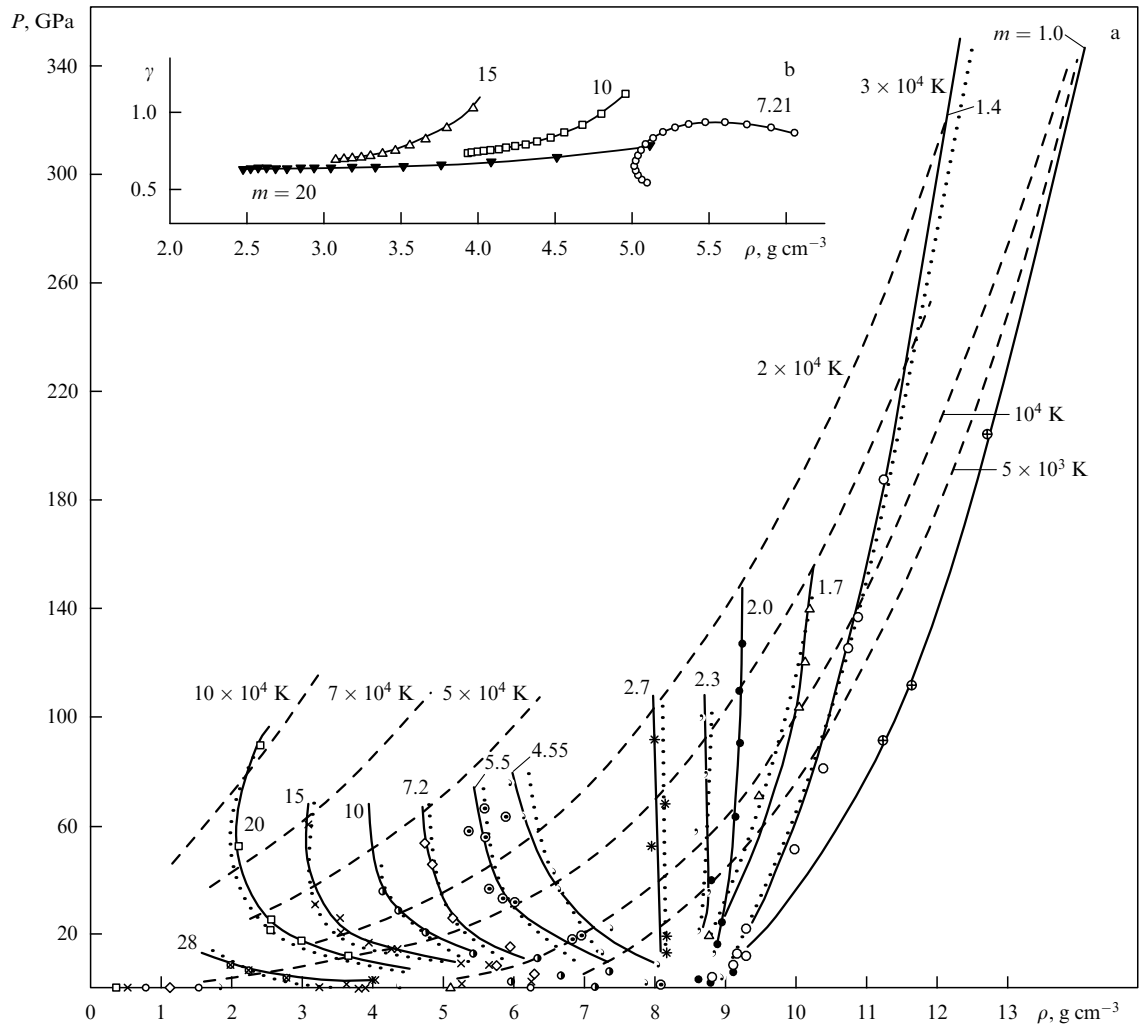

Figure 10. (a) $P-\rho$ diagram for nickel for different m: the solid lines are experimental shock adiabats, the dotted lines are adiabats calculated according to [20], the dashed lines represents isotherms calculated in [20] (the figures at the isotherms mark the corresponding temperatures). (b) Dependence $\gamma(\rho)$ along the adiabats for different m (according to [20]).

relate to changes of an electronic analog of the Grüneisen coefficient γ_e:

$$\text{at} \quad \left(\frac{\partial P}{\partial \rho}\right)_H > 0 \ (\text{for} \quad \rho > \rho_0)\,, \qquad \frac{\Delta P_H}{\rho \Delta E_H} = \frac{2}{m\sigma - 1} > \gamma_e\,;$$

$$\text{at} \quad \left(\frac{\partial P}{\partial \rho}\right)_H < 0\,, \qquad \frac{2}{m\sigma - 1} < \gamma_e\,;$$

$$\text{at} \quad \left(\frac{\partial P}{\partial \rho}\right)_H = \infty \ (\text{for} \quad \rho \approx \rho_0)\,, \qquad \frac{2}{m\sigma - 1} = \gamma_e$$

(this value corresponds to the shock-compression density limit).

So, by inspecting the forms of the shock adiabats, one can qualitatively analyze the variations of γ_e.

Now, let us look how the variation of the mean Grüneisen coefficient $\bar{\gamma}$ changes along adiabats with relatively large m. The corresponding data for nickel are shown at the top of Fig. 10. The main peculiarity of the dependences obtained is the equal asymptotic value at comparatively low densities ($\gamma \approx 0.65$). As for the individual (for each m) inconstancy of γ at small densities, it is explained by a strong sensitivity of the derivative $(\partial P/\partial E)_V$ to the small oscillations of the adiabat parameters at low densities.

Note that the estimate of the average Grüneisen coefficient $\bar{\gamma} = V(\Delta P/\Delta E)_V$ (ΔP and ΔE are the differences of the densities and energies for a fixed V in two adiabats of porous metals) for nickel is similar and is about 0.5. However, such estimates are not reliable enough, since the form of the compression curves makes it not always possible to find even two adiabats with the same volume. For the same reason it is impossible to do this over a wide range of the shock wave parameters. So, Ref. [27] suggested using the coefficient $\eta(P) = P(\Delta V/\Delta E)_P$. The advantage of using this coefficient for the description of the porous-material adiabats directly results from its form: it is derived from comparing adiabats at $P = \text{const}$, which allows it to be determined using any pair of adiabats. The connection between coefficients γ and η is as follows:

$$\eta(P) = \frac{P\gamma(\rho)}{\rho c^2 - P\gamma(\rho)}\,,$$

where c is the sound velocity. As shown in [27], the coefficient $\eta(P)$ for copper derived from adiabat comparison can be described by a single dependence. The same correspondence is also obtained from experiments with silica [28] and snow [29]. Using the equation of state

$$E(P, V) - E_1(P) = \frac{P}{\eta(P)}\left[V - V_1(P)\right],$$

these papers were able to describe the shock compression adiabats (including samples of various porosity) differing by orders of magnitude in their temperature characteristics. However, it was obvious that all data could hardly be presented by such a simple equation. The calculation data analysis revealed that this was indeed the case; in most cases, the equation leads to greatly overestimated values of the initial Grüneisen coefficient (and consequently to incorrect relations between the thermal components of densities and energies) and did not provide the correct asymptotics during the transition to the critical states. In addition, the requirement that the coefficient η be independent of other (apart form the pressure) parameters was not always duly satisfied. For example, the determination of this coefficient from the titanium shock compression dataset [30] did not lead to a single $\eta(P)$ dependence. In other words, this equation can be applied mainly in the region of high densities and pressures. Thus, we should use other more complex and informative semiempirical equations of state for a broad description of the thermodynamic parameters of materials. Now, we consider two such equations.

In the first case, the equation of state is written in the trinomial form [10]:

$$P(\rho, T) = P_c(\rho) + P_{tp}(\rho, T) + P_{te}(\rho, T)\,,$$

$$E(\rho, T) = E_c(\rho) + E_{tp}(\rho, T) + E_{te}(\rho, T)\,.$$

The first terms in these equations, $P_c(\rho)$ and $E_c(\rho)$, characterize 'cold' elastic atomic interactions for the temperature $T = 0$ K. The second and the third terms are associated with thermal vibrations of atoms (phonons) and electrons, respectively:

$$E_c(\rho) = \int_{\rho_0}^{\rho} P_c(\rho)\frac{d\rho}{\rho^2}\,; \quad E_{tp} = C_V T D\left(\frac{\Theta}{T}\right);$$

$$P_{tp} = \rho\gamma_p C_V T D\left(\frac{\Theta}{T}\right); \quad E_{te} = 0.5\beta T^2\,;$$

$$P_{te} = 0.5\rho\gamma_e\beta T^2\,; \quad \gamma_e = \frac{d\ln\beta}{d\ln\rho}\,.$$

Here, P is the pressure, ρ the density, $E(\rho, T)$ the specific internal energy, $E_c(\rho)$ the 'cold' energy (at $T = 0$ K), T the absolute temperature, C_V the lattice thermal capacity (for sufficiently low temperatures $C_V = 3R/A$, R is the gas constant, A the atomic mass), $D(\Theta/T)$ is the Debye function, γ_e the Grüneisen coefficient for electrons, and β the electron thermal capacity coefficient.

Estimates show that at megabar pressures the shock compression temperatures exceed, as a rule, the melting temperatures of a metal even on the solid-line adiabats. This is even more relevant to temperatures on the adiabats of porous materials, for which the heatings are very much higher. In this case, it is inappropriate to describe material properties by solid-state models. Here, it is necessary to take into account the temperature change in the lattice thermal capacity (from $3R$ at several Debye temperatures to $3R/2$ typical of a superheated liquid) and in the Grüneisen coefficient γ_p (from the corresponding value at a given density and $T \approx 0$ K to 2/3 at $T \to \infty$). These changes were first taken into account in [22]. The temperature dependences were simultaneously accounted for by analyzing experimental shock compression data for porous metals. In [22] the transitions to the limiting thermal capacities and Grüneisen coefficient were done using the coefficient

$$Z = \frac{lRT}{C_c^2}\,,$$

$$C_V = \frac{3}{2}\left[1 + (1 + Z)^{-2}\right]R\,,$$

$$\lambda = \frac{2(3\gamma_p + Z)}{3(2 + Z)}\,,$$

$$P_{tp} = \frac{RT(3\gamma_p + Z)}{(1 + Z)V} \quad \left(V = \frac{1}{\rho}\right),$$

$$E_{tp} = \frac{3RT(2 + Z)}{2(1 + Z)}\,.$$

Here, the Grüneisen coefficient γ_p (of the lattice) is expressed through the 'cold' sound velocity C_c:

$$\gamma_p = \frac{1}{3} + \frac{d \ln C_c}{d \ln \rho} .$$

Obviously, at $Z = 0$ the equations for P_p and E_{tp} turn into the Mie – Grüneisen equation for a solid body with $C_V = 3R$ and $\lambda = \gamma_p$, and as $Z \to \infty$ they turn into the gas equation $PV = RT$ with $C_V = 3R/2$ and $\lambda = 2/3$. For intermediate values of Z, the effect of the temperature (and density ρ through C_c) on P_{tp} and E_{tp} is in Z itself.

Let us say a few words about thermal electronic terms. Up to relatively low temperatures (about 30 – 50 thousand kelvins) [10, 11, 22], thermal electronic terms can be applied in the above form (with a quadratic dependence on temperature). But at higher temperatures the electron degeneracy disappears and the temperature dependence becomes almost linear. V D Urlin (see [22]) suggested using the following interpolation function for electronic terms

$$E_{te} = \frac{b^2}{\beta} \ln \cosh \frac{\beta T}{b}$$

(b is the adjusting parameter). At low temperatures this expression transforms into a quadratic function of temperature, and at high temperatures ($T > 50 \times 10^3$ K) tends to a linear dependence due to the coefficient b. Accordingly, the pressure is $P_{te} = \gamma_e \rho E_{te}$.

The 'cold' terms of the equation of state in [22] are assumed as a series in the degree of compression $\delta = \rho/\rho_{compr}$:

$$P_c = \sum_i a_i \delta^{1+i/3} , \quad i = 1, 2, \ldots, 7 .$$

The series coefficients can be found from the initial compression data, selected parameters on the shock adiabat of the solid metal, and from the 'cold' compression pressures on the calculated Thomas – Fermi high-pressure adiabats.

Finally, we show the way of taking into account the liquid phase in the equation of state. The corresponding transition algorithm is given in [31], which assumes the liquid equation-of-state parameters to be different from those of the solid phase by having an additional term containing an empirical function of density and temperature. The constants of the additional term can be determined from the description condition of the experimental melting curve. The curve itself is found from the minimization of the Gibbs potential. The equation of state with several free parameters allows a satisfactory description of the entire experimental dataset on the shock compression of materials.

The equation which consistently considers temperature effects on the thermodynamic parameters of a compressed material was first studied in [22]. Various variants using simplified or, conversely, complicated forms of equations appeared later on. Omitting the description of these modifications, let us only mention the main approaches in some of them. First of all (and this is one of the primary achievements in the further improvement of equations), this is the expansion of the description of thermodynamic properties in the region $\rho < \rho_0$, where the equation considered in [22] is inapplicable. The approach accepted in [32 – 34] and in some other papers suggests defining the dependences $P_c(\rho)$ over the entire range $0 < \rho < \rho_0$ with a minimum at $(dP_c/d\rho) = 0$ and $\gamma_p(\rho)$ changing from the value of γ_p at ρ_0 to $\gamma_p = 2/3$ at $\rho = 0$. This allows at least a qualitative description of the two-phase liquid – vapor region. The form of terms (in particular, electronic terms) in certain equations [32, 33] is simplified. The general description of experiments has not worsened. Note that all mentioned models were elaborated for solid state. For transition to the liquid-state description, additional terms taking into account melting at the wave front are required.

Since the region of liquid state largely exceeds that of solid state, it appeared logical to consider the construction of the equation of state using the liquid model. This approach was used, in particular, in [20]. Recall that the model was first suggested long ago by van der Waals:

$$P(V, T) = P_{rep} + P_{att}(V) = \frac{RT}{V - V_c} - \frac{A}{V^2} . \tag{6.1}$$

Here, P_{rep} and P_{att} are the 'repulsion' and 'attraction' pressures, respectively, A is the constant of attraction, V_c is a constant called the covolume, and R is the gas constant.

It is presumed in [20] that the only factor that forces the material to be compressed is pressure; therefore, $V_c = V_c(P_{rep})$. Further, for convenience one uses the inverse function $P_{rep}(V_c)$. Then, in variables T and C_c the equation of state reads as

$$V = V_c + \frac{RT}{P_{rep}(V_c)} , \tag{6.2}$$

$$P = P_{rep}(V_c) + P_{att}(V) . \tag{6.3}$$

The free energy F of the model, which determines the entropy $S = (\partial F/\partial T)_V$, the internal energy $E = F + TS$, and other thermodynamic parameters, is

$$F = R\varepsilon_0 + E_{rep}(V_c) + E_{att}(V) + \frac{3}{2} RT - RT\left[S_0 + \frac{5}{2} \ln T - \ln P_{rep}(V_c)\right] , \tag{6.4}$$

where

$$E_{rep}(V_c) = -\int_{V_0}^{V_c} P_{rep}(V_c)\, dV_c ,$$

$$E_{att}(V) = -\int_{V_0}^{V} P_{att}(V)\, dV , \quad \varepsilon_0 = \text{const} , \; S_0 = \text{const} .$$

The model takes into account the compression of the liquid at low temperatures and its evaporation. This corresponds to the limiting states (as $T \to \infty$, it passes into the equation of state of a perfect gas). To describe high-temperature states with ionization, the model admits generalization (see [20] for the corresponding algorithm).

For a mixture of ions and electrons, the free energy is expressed in the form:

$$F = E_{rep}(V_c) + E_{att}(V) - RT \sum_k a_k \ln \frac{a\sigma_k(T)}{a_k P(V_c)} , \tag{6.5}$$

$$V = V_c + \frac{aRT}{P_{rep}(V_c)} . \tag{6.6}$$

Here, k is the particle sort index, a_k is the particle concentration ($a = \sum a_k$), and $\sigma_k(T)$ is the partition function of particles of the kth sort. For electrons, $k = \text{e}$; for ions, $k = \text{i}$. Then, at thermodynamic equilibrium the values a_i and a_e are obtained from the solution of equations

$$\mu_i = \mu_{i+1} + \mu_e \quad (\mu \text{ are chemical potentials}).$$

The substitution of chemical potentials from (6.5) and (6.6) into this expression yields the system of Saha's equations (as $V \to \infty$).

In order to obtain the equation of state in the form (6.1)–(6.5), empirical functions with a certain number of free parameters should be known. In [20], such functions were chosen in the form of simple power (or power series) or exponential expressions. The characteristics of ions from (6.5) are assumed to be equal to those of gas.

In the region of solid states, the Mie–Grüneisen model is used:

$$P = P_c(V) + \gamma(V)\,\frac{3RT}{V}\,,$$

$$E = E_c(V) + 3RT\,.$$

It is assumed that the Grüneisen coefficient is $\gamma(V) = \gamma_0(V/V_0)$, and P_c and E_c are the 'cold' (taken at $T = 0$ K) pressure and energy.

Reference [20] suggests the following procedure for transition from the solid phase to liquid. With given equations of state for the liquid and solid phases, the following phase equilibrium conditions are met along the melting line:

$$P_l = P_s\,, \quad T_l = T_s$$

and the Gibbs thermodynamic potentials are

$$(F + PV)_l = (F + PV)_s\,.$$

This results in the Clausius–Clapeyron equation

$$\left(\frac{dT}{dP}\right)_{\text{melt}} = \frac{V_l - V_s}{S_l - S_s}\,.$$

It is accepted further that along the melting boundary the following condition should be fulfilled:

$$\frac{V_l - V_c}{V_c} = \beta = \text{const}\,,$$

where β is an empirical parameter. This condition in combination with Eqn (6.1) determines the melting line on the T–P plane.

The model contains several free parameters, which are selected using data on the shock adiabat of the continuous material, the temperature and enthalpy under natural conditions (reference data), and the binding energy. The model was applied for description of the shock-compression experiments for many metals without reference to the shock compression of porous samples and showed good agreement between calculations and experimental results. As an illustration, in Fig. 10a we show shock adiabats for nickel described by this model.

7. Additive relations for shock adiabats

We will follow the following postulate: the shock adiabats for complex materials are presumed to be equivalent to the equilibrium mixtures of their individual components (elements, oxides, etc.). According to [35–38], for some 'mixed' compositions, estimates of the shock-adiabat positions on the P–V plane can be obtained applying the rule of additivity of specific volumes (under equal pressures) for individual compounds that constitute the mixture according to their stoichiometric relations. Strictly speaking, this rule can be applied to isothermal processes, when the separate components of the mixture studied acquire both equal pressures and temperatures. The pressure, temperature, and specific volume $V = \sum_i \alpha_i V_i$ are thermodynamic variables. Here, α_i are the weight fractions of the components ($\sum_i \alpha_i = 1$).

The use of the additive approximations shows that to find shock adiabats in many cases it is sufficient to simply add the specific volumes on the shock adiabats of the initial structures without passing to their isothermal compression curves, which greatly simplifies the calculations. Satisfactory results obtained with such an approach are apparently explained by the small difference in the equations of state of the individual components. Below, for whole classes of materials we will use exactly this procedure.

7.1 Compression of metal alloys

Belyakova et al. [36] considered the shock compression of 47 metal alloys from three main groups differing by the type of interatomic bonds: chemical compounds (7 materials), mechanical mixtures (9), and solid solutions (14). In addition, the results of studies for multicomponent groups were analyzed, with a special attention given to Fe and Al alloys. The additive dependences were always calculated with initial adiabats of elements taken from [12].

Figure 11a illustrates the comparison of the calculated additive curves with experimental data. The analysis of the results [36] implies good agreement between the calculations and experimental data. The exception is for two (not plotted in the figure) chemical compounds: Fe–Si (the difference in density at maximum pressures reaches 15%) and Ti–Ni (6%). This discrepancy is not removable. With the use of the calculated adiabats for high-density phases of Si and Ti, the discrepancy still exceeds experimental errors.

These and other small deviations indicate that

— the difference in the calculated description and experimental data mainly has a close percentage deviation and the same sign as the difference in the initial alloy densities (their experimental and additive values);

— most of the deviations refers to alloys consisting of elements differing from each other only by their atomic numbers in the periodic table;

— only chemical compounds have deviations exceeding measurement errors; alloys (mechanical mixtures and solid solutions) are satisfactorily described by additive relations.

7.2 Compression of metal carbides

In the D–U coordinates, the initial parts of the shock adiabats for metal carbides [37] correspond to $D \approx$ const and even to a decrease (!) of wave velocities with increasing mass velocities (TiC and WC in Fig.12). At the same time, the critical value of D for $U \to 0$ does not contradict the bulk sound velocity, which implies the reliability of the data obtained at small wave parameters.

The reasons for such a velocity decrease are unclear. Experiments with thick samples and continuous registration of the shock-wave parameters (e.g., mass velocities) could probably shed light upon its nature.

The transition of carbon into the diamond phase can most probably occur under such conditions. So, concerning the second parts of the carbide adiabats, this specific process could exert a certain effect on them. This fact is indicated by good consistency between the upper branches of adiabats of carbides with an additive mixture of diamond [39] and the

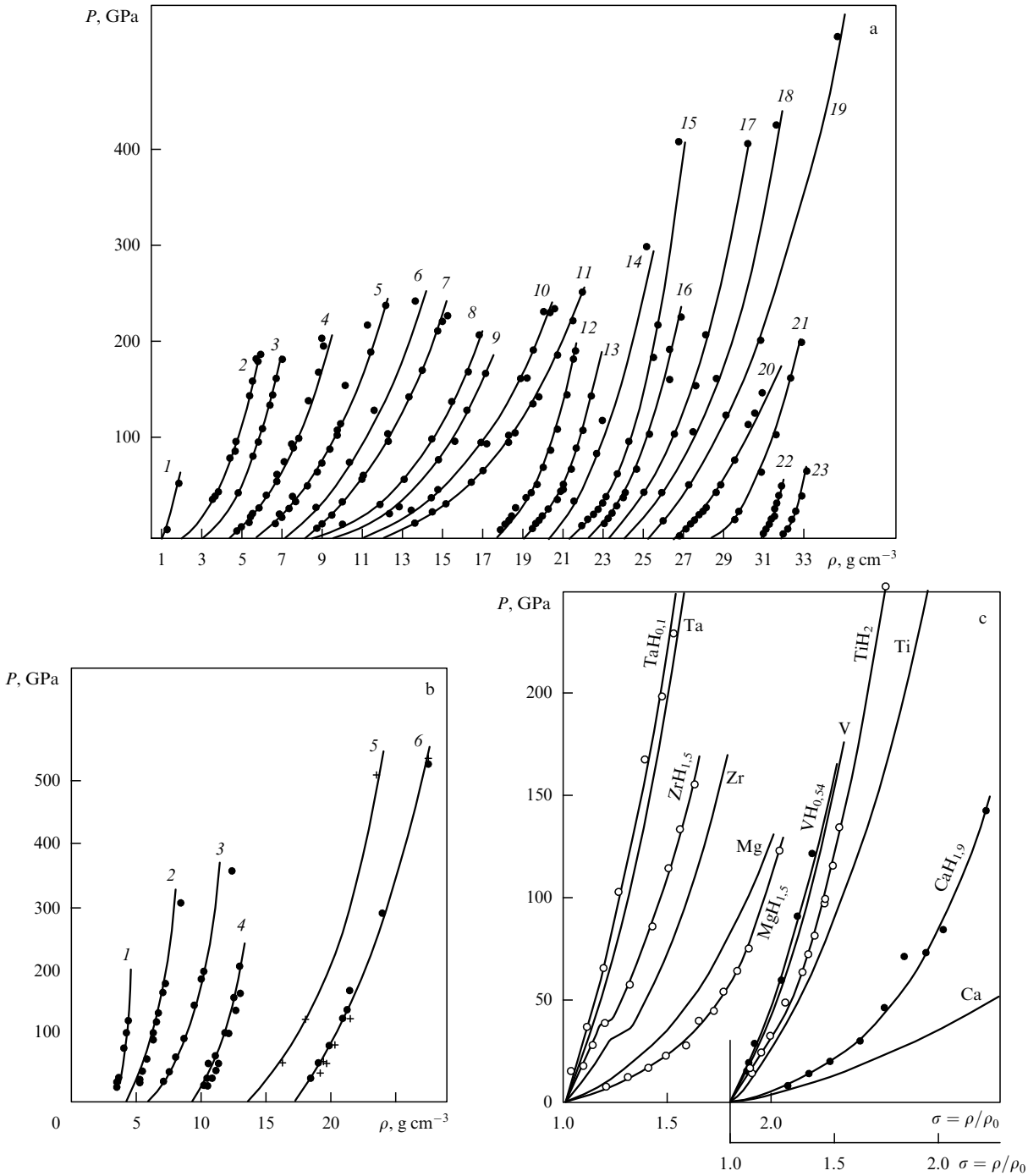

Figure 11. Shock adiabats for metallic alloys: *1*, Be(68%) – Al(32%); *2*, Fe(90%) – Ni(10%); *3*, Fe(74%) – Ni(26%); *4*, Cu(74,5%) – W(25.5%); *5*, Cu(45%) – W(55%); *6*, Cu(32%) – W(68%); *7*, Cu(24%) – W(76%); *8*, Au(90,7%) – Ge(9.3%); *9*, Au(92.1%) – Ge(7.9%); *10*, U(86.6%) – Rh(13.4%); *11*, U(91,7%) – Mo(8.3%); *12*, Fe(60%) – Co(40%); *13*, Fe(90%) – W(10%); *14*, Ti(70%) – Mo(30%); *15*, Fe(49%) – Cu(51%); *16*, Ni(50%) – Cu(50%); *17*, Ta(5%) – Nb(95%); *18*, Ta(30%) – Nb(70%); *19*, Re(60%) – Mo(40%); *20*, Ti(34.3%) – Zr(65.7%); *21*, Co(64.5%) – Ni(35.5%); *22*, Mg(85%) – Li(14%) – Al(1%); and *23*, Mg(88%) – Li(12%). (b) $P-\rho$ diagram for carbides of metals: *1*, SiC; *2*, TiC; *3*, ZrC; *4*, NbC ($\rho+2$); *5*, TaC; and *6*, WC ($\rho+2$). (c) The comparative compressibility of hydrides and metals forming them.

corresponding metals [12]. This is illustrated in Fig. 11b, which compares the additive calculations (using initial adiabats) with experiment.

7.3 Compression of metal nitrides

The shape of the shock compression adiabats for metal nitrides are qualitatively similar to those for carbides. In the $D-U$ coordinates, the first parts are either fitted by straight lines ($D \approx$ const), or characterized by a wave velocity decrease with increasing mass velocities (see Fig. 12). The second parts of the adiabats for nitrides are represented by steep, weakly compressed parts of the dense phases of these compounds.

Note one peculiarity of nitrides. The initial density of many of them exceeds the density of the corresponding metals; a sort of compaction occurs due to nitrogen

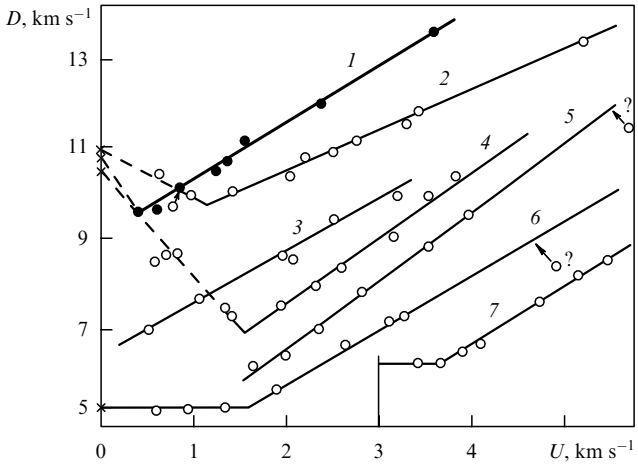

Figure 12. $D-U$ diagram for carbides and nitrides of metals: *1*, WC ($D+4$); *2*, TiC ($D+1$); *3*, TiN; *4*, AlN; *5*, ZrN ($U+1$); *6*, ZrC ($D-2$); and *7*, NbC ($U+3$).

'absorption' by the metal. The specific volume of many nitrides is smaller than that of their components, which contradicts the main rule of additivity of volumes. We refer to that type the following nitrides studied: AlN, Si_3N_4, and TiN. TaN is the only of the nitrides considered in [37] whose specific volume lies between those of nitrogen and tantalum. But even its calculated additive dependence disagrees with experiment. The same is the case for ZrN.

So, metal nitrides provide an example where the additive approximation fails even in principle.

7.4 Compression of metal hydrides

Hydrides were the last class of metal compounds studied. Some of them play an increasingly important role in various fields of high-density engineering, which explains the great attention the scientific community pays to their studies.

In addition to the general physical interest in the studies of the new specific class of compositions (metal–hydrogen) under intensive pulse loadings, there is another reason for the interest in this research. It is related to the possibility of testing Larin's hypothesis [40] about the hydride structure of planets of the Earth group. According to this hypothesis, the high density of the Earth's internal core is explained by the strong compressibility of metal hydrides due to strong deformation of hydride ions. The state of the effectively liquid external core is related to the significantly enhanced mobility of atoms of metals on their saturation with hydrogen at the high temperatures of the Earth interiors.

Direct experimental data on the compression of hydrides allows verification of the main assumption of the hypothesis on the anomalously high compression of metal hydrides. The peculiarity of the compositions under consideration, as well as of nitrides, is the ability of metals to be 'saturated' by hydrogen. At the same time some of them (in particular, alkaline and many alkaline-earth metals) are strongly compressed and their initial density exceeds that of the initial metal. The results of studies of the compression of hydrides of calcium, magnesium, titanium, zirconium, vanadium, and tantalum are collected in [41]. By the nature of metal–hydrogen bond, most of them refer to metallic hydrides, calcium hydride is ionic, while magnesium hydride corresponds to an intermediate type between ionic and covalent compounds.

Figure 11c shows experimental data and compares them with the location of the corresponding metals on the pressure–compression plane. The transition metals and their hydrides have a similar character of compression. At pressures about 200–250 GPa, their location difference does not exceed 6% in density. The compression of metal can be both larger and smaller than the compression of the corresponding hydride. For light metals (Li, Ca, Mg), the compression of hydrides is usually less than that of metal.

The main conclusion from the experimental results is that the compression of metal hydrides is not accompanied by an anomalous density increase. Although the number of hydride compounds considered here is not large, there are hardly grounds to believe that one can find other hydrides with highly different properties.

So the assumption of Larin's hypothesis of an enormously high compression of metal hydrides is not supported. Generally, the rule of additivity of specific volumes cannot be applied to metal hydrides, which is in particular due to the hydrogen 'saturation' effect in metals that increases their initial density.

8. Minerals

By the type of chemical bond between structure units, minerals from inorganic groups are usually separated into four broad classes: oxides, oxygenic salts, halogenides, and native elements (including already mentioned metals). In this section, we will consider the compression of minerals only from these classes.

8.1 Oxides

8.1.1 The shock compression of silica. Of all the oxide structures employed in shock compression experiments, silica has been studied most completely (in its different phase modifications) both over a wide pressure range (from laboratory studies to underground nuclear explosion experiments) and with the use of various methods. In the last four decades, the shock compression has been studied for α quartz, quartzite (polycrystal form of quartz), coesite, cristobalite, and amorphous quartz. Besides, twofold compression of quartzite, its expansion adiabats, etc. have been investigated. There are several reasons for such attention to SiO_2.

1. Silica is a widespread rock-forming mineral and at the same time is an original rock as well.

2. Silica is a 'multiphase' system. Seven different modifications are known. It would undoubtedly be interesting to trace the sequence of shock-induced silica transformations.

3. High-density silica modifications (like stishovite) play a special role in the composition of the internal layers of our planet. It is generally recognized that stishovite is the main constituent of the Earth's mantle. But there are more advanced hypotheses, speculating that the Earth's core consists of superdense phases (with a density higher than stishovite's) of silica.

Shock waves allowing one to obtain pressures significantly exceeding those in the center of the Earth represent a powerful tool for geophysical studies of oxides and minerals.

8.1.2 Silica compression measurements. The first Russian paper which considered the compression of α-SiO_2 appeared in 1960 [42]. Already in this paper, an interesting effect was discovered. At pressures of $\sim$100 kbar, a density jump was detected in the compression curve of quartz, which was

explained in [42] as an α quartz ($\rho_0 = 2.65$ g cm^{-3}) – coesite ($\rho_0 = 2.98$ g cm^{-3}) phase transition. However, this interpretation proved to be wrong. Wackerle [43], who studied α-SiO_2 in the same pressure range, also detected a phase transition, but, based on a more careful experiment, another explanation to its nature was suggested, namely, as an α-SiO_2 – stishovite transition ($\rho_0 = 4.28$ g cm^{-3}). Later on, this treatment became generally accepted.

The megabar interval of compression studies for quartz was overcome in 1965 [44]; in 1971, the pressure threshold was raised to 350 GPa for laboratory conditions and to 550 GPa (quartzite) for underground nuclear explosions [45].

The comparative compressibility of the Al – SiO_2 system was measured up to 2 TPa [45]. Later on (1980), this pressure was raised to ~13 TPa [46], the record value for the relative compression of quartz.

Between 1971 and 1990, the compressibility of porous quartz, twofold compression (by two consecutive waves), the expansion adiabat, and the compressibility of various phases of silica (cristobalite, amorphous quartz, coesite) were studied [47 – 51]. We will not consider the results of measurements of various parameters of quartz compression in the region of its phase transition (or transitions), because there are more than twenty publications devoted to this problem and the subject is worth discussing separately. We will only consider the silica shock compressibility data that refer to the superdense branch on the shock adiabat.

In Figure 13a, we display the joint results of compression measurements of α quartz (single-crystal samples, $\rho_0 = 2.65$ g cm^{-3}), quartzite (polycrystalline samples, $\rho_0 = 2.65$ g cm^{-3}), coesite ($\rho_0 = 2.92$ g cm^{-3}), amorphous quartz ($\rho_0 = 2.2$ g cm^{-3}), and cristobalite ($\rho_0 = 2.13$ g cm^{-3}), as well as the results for quartzite obtained in underground nuclear explosions. The main difference of the latter from the laboratory measurements is the use of significantly thicker samples (by two orders of magnitude). The thickness of laboratory samples was several millimeters, while in underground explosions it reached 1 meter. So, the coincidence of both results indicates that the shock-wave front plays a special role in the phase-transition kinetics: the formation of the new phase takes place mainly at the shock front and does not depend on the experiment scale. This conclusion was of great importance both for the studies of phase-transition kinetics and for the solution of some technical issues.

Another important conclusion is that after the α-quartz – stishovite phase transition, the experimental adiabat for quartz (quartzite) up to a pressure of 13 TPa (the shock velocity $D \approx 37$ km s^{-1}) shows a smooth, monotonic behavior without new mass-velocity jumps, i.e., without density jumps. This complicates the construction of the Earth-core models based on superdense silica phases but does not completely exclude such a possibility.

The reason for lack of a denser-than-stishovite silica modification could be the strong shock heating of silica. Perhaps, the decrease of its temperature using another compression regime or direct studies of the compression of stishovite samples could handle this problem. These direct experiments with stishovite are of special interest. However, these measurements have not yet been performed due to the technical difficulties in obtaining samples of appropriate sizes for such experiments.

8.1.3 Compression of porous silica. The conclusion that the phase transition in silica is indeed α-SiO_2 – stishovite is based

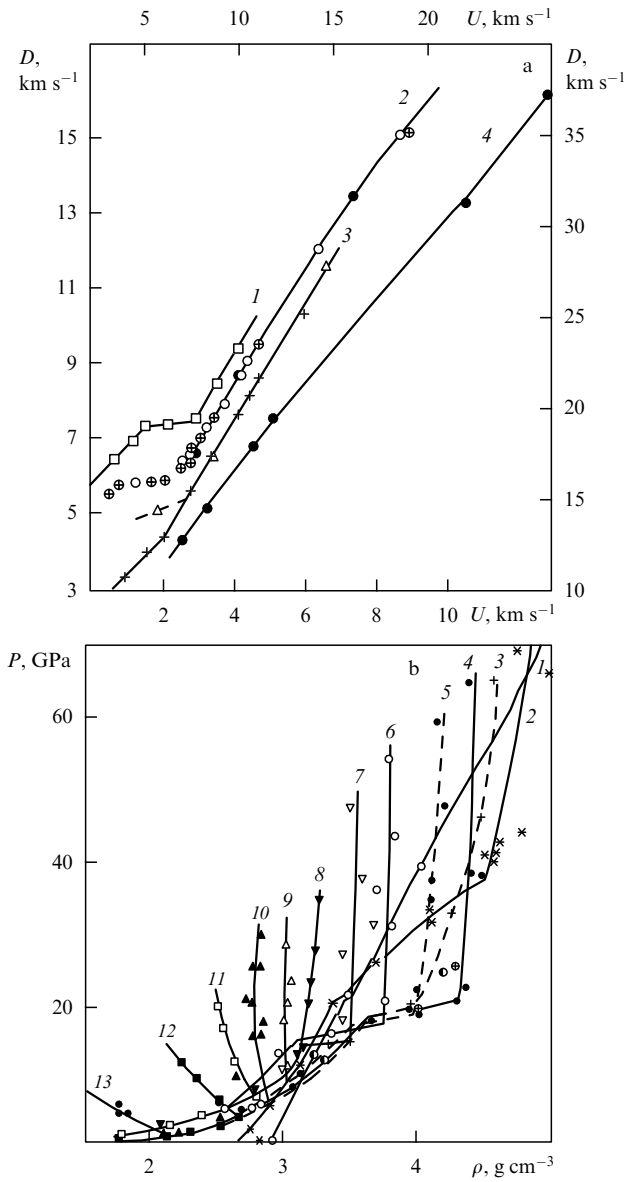

Figure 13. (a) $D - U$ diagram for silica: ⊕, α-quartz; ○, quartzite; ●, quartzite (measurements in underground nuclear explosions); *1*, coesite, *2 – 4*, quartz – quartzite (scales for dependence *4* are on the right and on the top), *3*, amorphous quartz (+) and cristobalite (Δ). (b) $P - \rho$ diagram for silica: *1*, the shock adiabats for coesite ($m = 1,0$); *2*, α quartz (quartzite); *3*, cristobalite ($m = 1.22$); *4 – 13*, porous α quartz with initial densities 1.75, 1.55, 1.35, 1.15, 0.8, 0.65, 0.55, 0.40, 0.20, and 0.13 g cm^{-3}, respectively.

in [43] on the agreement between the value of density obtained from the extrapolation to $P = 0$ of the steep branch of quartz adiabat and the stishovite density. The correctness of this conclusion could be verified by studying the shock compression of quartz with various initial densities ('porous' quartz). If the quartz – stishovite transition really takes place, then the 'porous' shock adiabats will form a fan of ascending superdense branches centered on the initial density of stishovite. As always, the reality turned out to be more complex and the nature of phase transformations in silica under shock loading have not yet been established. Incidentally, this assertion does not relate to the problem of transition of silica to stishovite (or a stishovite-like liquid), which was generally solved, in particular, in studies of porous samples. The results of these

measurements [47–51] are plotted in Fig. 13b. It is seen that data for silica can be, somewhat arbitrarily, classified into three groups. The first group consists of adiabats with the initial density $\rho_{00} > 1.55$. The extrapolation of the steep parts (dense phase) of the adiabats to $P = 0$ (bearing in mind the differences in the shock compression temperature) yields a density in good agreement with the initial density of stishovite. The mutual location of the curves from this group in the phase-transition region indicates the non-equilibrium of the detected states and the possibility of 'working up' of the high-density phase already after the formal completion of the phase transition. Note that the quartz–coesite transition, due to specific kinetics of transitions under way, can possibly be 'screened up' by the main 'stishovite' transition. The usual methods of detection do not allow us to identify shock-compression-induced SiO_2 phases. Only the last 'stishovite' chain of these transformations proves detectable (and even not in a direct way).

Perhaps, an additional reason for the difference between stishovite density and the density obtained from the extrapolation of the steep branch of the adiabat to $P = 0$ is the nonequilibrium of states.

The compression curves with $0.06 < \rho_{00} < 0.8$ g cm^{-3} may be associated with coesite adiabats. The extrapolation of their high-density parts to zero pressure does not contradict the initial density of coesite ($\rho_0 = 2.98$ g cm^{-3}). Finally, there are three adiabats ($\rho_{00} = 1.15$; 1.35, and 1.55 g cm^{-3}) between the adiabats we associate with coesite and stishovite.

Let us enumerate some qualitative conclusions which can be inferred from an analysis of the compression data for porous silica.

1. As the initial materials, experiments [47–51] used various substances equivalent to silica in composition and content: anhydrous silicic acid ($\rho_{00} = 0.55$; 0.65, and 0.8 g cm^{-3}), aerosil ($\rho_{00} = 0.2$; 0.4, and 0.55 g cm^{-3}), α-SiO_2 ($\rho_{00} = 1.15$; 1.35; 1.55, and 1.75 g cm^{-3}), cristobalite ($\rho_{00} = 2.13$ and 1.15 g cm^{-3}), and coesite ($\rho_{00} = 2.4$ g cm^{-3}).

As a rule, separate shock adiabats are obtained using one composition of silica. This is due to the fact that some of the initial densities can only be produced from one composition (others had inappropriate density when pressing the samples). But sometimes the possibilities overlapped, so some control points were determined using different silicas. The coincidence of the final results was good; i.e., for a given ρ_{00} there was a single shock adiabat of silica, irrespective of the initial compositions.

2. For adiabats along which the compression leads to phase transitions to a dense phase (stishovite, $\rho_{00} \geqslant 1.75$ g cm^{-3}), the pressure at which the transition mainly completes increases with the initial density of the sample. For example, for coesite with an initial density of 2.92 g cm^{-3}, the pressure is ~ 600 GPa, while for α-SiO_2 with $\rho_{00} = 1.75$ g cm^{-3}, it is 20 GPa. A similar rule holds for transitions to the coesite state. For the 'intermediate' adiabats ($\rho_{00} = 1.55$; 1.35, and 1.15 g cm^{-3}), the transition completes at nearly the same pressures about $\sim 17-18$ GPa.

3. For all 'stishovite' adiabats, the phase transition occurs with a density jump in the $D-U$ coordinates (a break in the mass velocities at $D \approx$ const). In the 'coesite' adiabats, the phase transition corresponds to a bend in the curve (change of slopes), i.e., to the presence of two parts of the adiabat.

4. The slopes of adiabats in the intermediate region between 'coesite'-like and 'stishovite'-like adiabats are essentially the same, i.e., their $P(\rho)$ dependences are parallel to each other.

5. Adiabates of materials with a 'coesite' composition can be represented as a fan of curves. The extrapolation of these curves to zero pressure does not contradict the initial density of coesite ($\rho_{00} = 2.92$ g cm^{-3}). Their slope $\mathrm{d}P/\mathrm{d}\rho$ changes from positive (for $\rho_{00} \geqslant 0.8$ g cm^{-3}) and $\mathrm{d}P/\mathrm{d}\rho \approx \infty$ ($\rho_{00} = 0.65$ g cm^{-3}) to negative ($\rho_{00} \leqslant 0.55$ g cm^{-3}).

6. The estimates of shock-compression temperatures demonstrate that the transition of silica to dense phases occurs mostly in the solid states.

To conclude the data analysis of the silica shock compression we consider its twofold compression.

8.1.4 Twofold silica compression. As mentioned above, the high shock-compression temperature prevented silica from transforming to denser modifications. The goal of silica twofold-compression studies is to try to investigate the phase transitions on the 'stishovite' shock adiabats for smaller (in comparison with a single compression) heating of the samples. The setting of experiments is essentially similar to that considered above in the reflection method (see Fig. 1), with the only difference being that here the material to be studied (quartz or quartzite) is used as a screen, behind which the samples of the 'heavy' standard metals ($\rho_0 > 7$ g cm^{-3}) are installed. In this case, the studied sample is compressed twice: the first time, by the direct shock-wave impact, and the second time, by the reflected wave from the standard metal. The shock velocities are registered in the quartz and in the metal samples. With the known shock adiabats of quartzite and metals, the states of twofold compression of quartz are calculated using the following relations:

$$P_2 = P_1 + \rho_1 D_{12}(U_1 - U_2)\,, \quad \rho_2 = \rho_1 \frac{D_{1,2}}{D_{1,2} - (U_1 - U_2)}$$

(D_{12} is the velocity of the second wave reflected from the obstacle relative to the states behind the first wave). Similar expressions hold during the phase transition on the twofold compression adiabat. In this case, P_2, ρ_2, U_2 are the parameters of the adiabat break points, respectively, and U_2 and D_{12} refer to the phase transition region and correspond to parameters U_3 and D_{13}. The data obtained were published in [53].

The final results are illustrated in Fig. 14a. Obviously, the twofold compression adiabats have bends which can be considered as an indication of the stishovite transition to a new superdense phase. Unfortunately, the steep branch corresponding to the new phase, is not fixed in the considered experimental setting. To fix it, new methods of second-wave formation with an amplitude independent of the first one are required.

So, twofold quartz-compression experiments point to the possible existence of a denser-than-stishovite phase of SiO_2. Note, however, that the accuracy of registration of the twofold compression parameters by this method is not high. For the extreme variations of the initial parameters and measurement errors of the kinematic parameters, the twofold compression can be described without obvious bends. This urges direct studies of the shock compression of stishovite as the original material. Recently published experimental data on stishovite [54], unfortunately, do not allow one to solve this problem due to the poor quality of

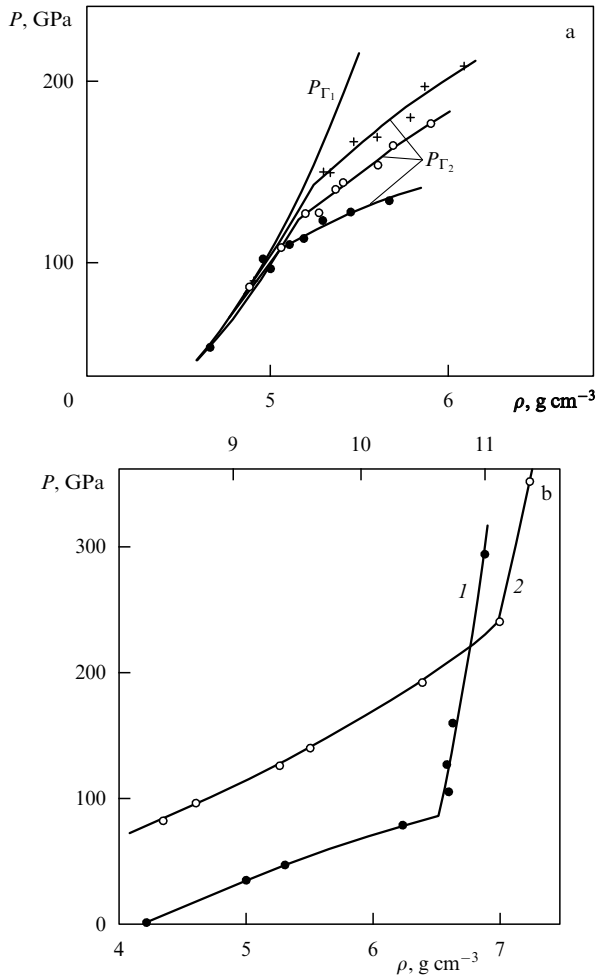

Figure 14. (a) Twofold shock compression adiabats for silica. (b) Shock adiabats for (*1*) rutile (the dark circles and the density scale in the bottom) and (*2*) cassiterite (the open circles and the density scale on the top).

sample manufacturing and insufficient registration accuracy. Experiments with precision samples and the traditional 1% accuracy of kinematic parameter determination are needed. In this case they could put an end to the old discussion about the possibility of existence of a denser-than-stishovite silica modification.

8.1.5 Compression of rutile and cassiterite [55, 56]. These oxides have the same initial structure (rutile-like, the coordination number c.n. = 6) as stishovite. It is natural to ask: How do other materials with the same structure behave in shock waves? Although they are characterized by a sufficiently dense packing of atoms in the lattice, is it possible in them to realize a transition into structures with c.n. > 6, for example, into the fluorite type (CaF_2) with c.n. = 8? The results of experiments demonstrate (Fig. 14b) that it is quite possible. Under the shock compression, rutile transforms with a 1.5 times increase and SnO_2 with 1.7 times increase in the initial density. The examples considered also indicate, although indirectly, the possibility of existence of a denser-than-stishovite phase.

8.2 Oxygen salts [57 – 59]

Oxygen salts include the following experimentally studied materials:

— carbonates: calcite ($CaCO_3$), magnesite ($MgCO_3$), and dolomite ($CaMg(CO_3)_2$) [57];

— sulfates of barium ($BaSO_4$) and calcium [anhydrous ($CaSO_4$) and gypsum ($CaSO_4 \cdot H_2O$)] [58];

— silicates: topaz ($Al_2SiO_4[FO_4]_2$), enstatite ($MgSiO_3$), microcline ($K[AlSi_3O_8]$), beryl ($Be_3Al_2[Si_6O_{18}]$), etc. [58 – 59].

Some of the results obtained are shown in Figs 15a and 15b. Clearly, adiabats of minerals inside groups are close to each other both qualitatively and by the slopes of the second parts of the $D(U)$ dependences. Apparently, this is due to the similarity of the crystalline structures of the minerals inside a given group. Thus, silicate minerals have a common structural cell — silica – oxygen tetrahedron. Different 'packings' of such tetrahedra form simple and complex groups (radicals). The variety of the first parts of the adiabats might be associated with the different compressibility of radicals packed in different ways. After the repacking processes are completed and the silicates acquire the 'general compressed' structure, the adiabats become similar to each other. The similarity of the adiabats of minerals from other groups is also explained by the resemblance in their structures (initial or obtained during the compression).

8.3 Halogenides, sulfides

Of halogenides, the following compositions have been studied: Na_3AlF_2, CaF_2, BaF_2, NaCl, KCl, KBr, LiF, and CsBr. In addition, the sulfides ZnS and FeS_2 have been studied. On the shock adiabats of halogenides KCl and KBr [60, 61] at a pressure of $P \approx 2$ GPa, the phase transition of KCl and KBr into a CsCl-like structure with c.n. = 8 occurs. This transition was detected and studied by many Russian and foreign researchers with the use of different methods and became a sort of classic example of shock phase-transition registration.

Some uncertainty is associated with the phase transition in NaCl. Under static compression conditions, the phase transition in rock salt was detected at a pressure of 20 GPa [62, 63] by X-ray diffraction. However, dynamic tests [64, 65] did not give direct evidence of its existence from changes in the shock adiabats parameters, although some papers [65, 66] reported on deviations from monotonic compression curves.

Convincing proofs of the phase transition in rock salt were obtained in the underground nuclear explosions right inside a rock-salt deposit [67]. Summarized results of several tests are plotted in Fig. 16a in $D - t/r$ coordinates (t is the time, r is the distance to the explosion point). In these coordinates, the total data from different experiments are described by a single curve of the shock velocity change as a function of the reduced distance. Obviously, the $D(U)$ dependence has a rather complex form. The states corresponding to the initial phase and the regions of a two-phase mixture passing into a region of dense high-pressure phase and then to the zone of liquid are all fixed on this curve. After these results had been obtained, new precision experiments were performed, in particular in the region of wave velocities corresponding to the phase transition detected in the underground measurements. The results of these experiments demonstrate (Fig. 16b) that the phase transition in NaCl takes place even under the laboratory conditions (at about the same pressures as in static conditions).

Note that in underground explosions and for pressures above the phase transition (in the liquid region), a monotonic shock-wave decay is detected. This contradicts the results of Ref. [61], in which for NaCl, KCl, and KBr a zone of change

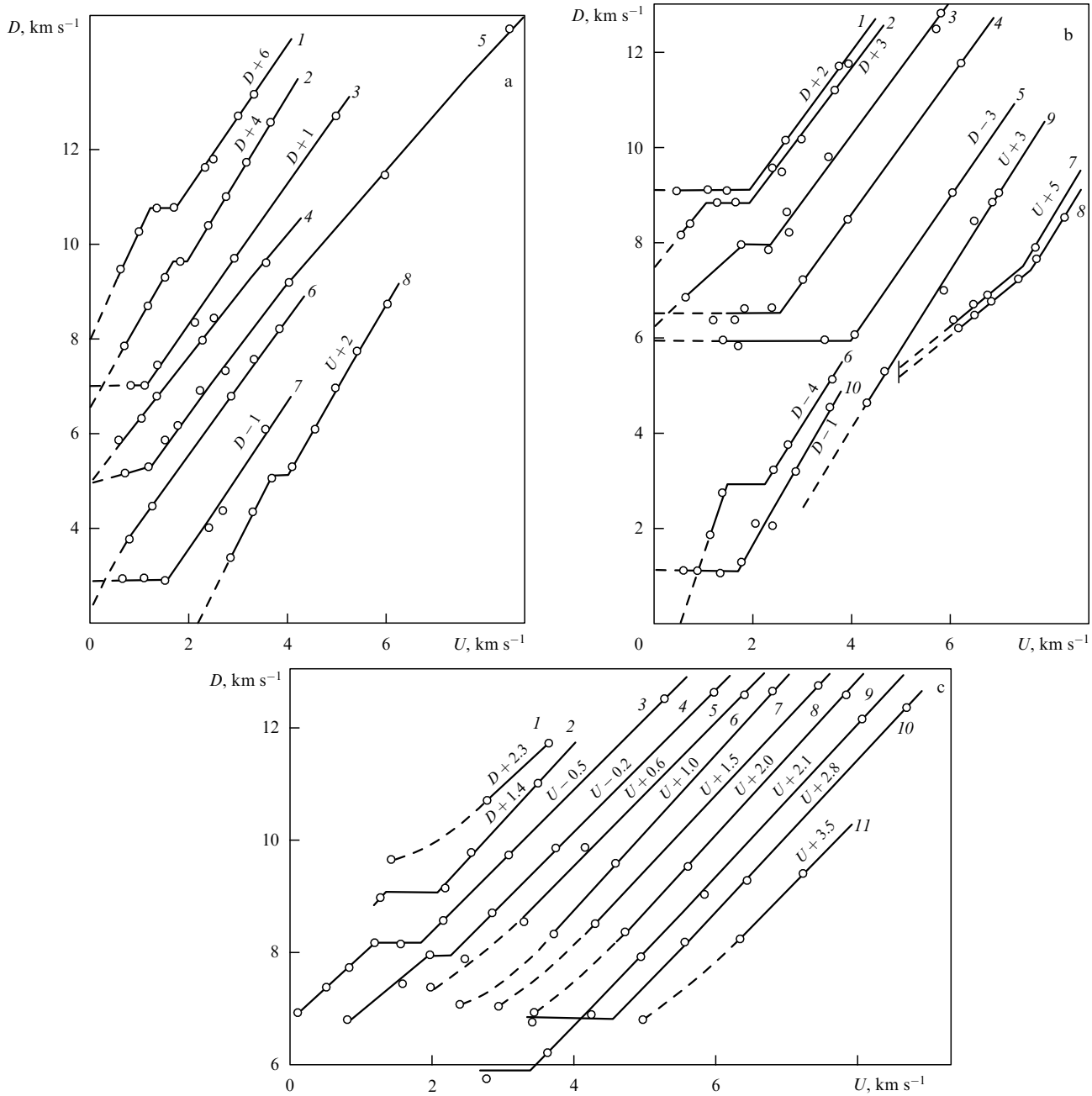

Figure 15. (a) $D-U$ diagram for carbonates, sulfates, and sulfides: *1*, $BaSO_4$; *2*, $CaSO_4$; *3*, FeS_2; *4*, $MgCO_3$; *5*, $CaMg(CO_3)_2$; *6*, $CaCO_3$; *7*, ZnS; and *8*, $CaSO_4 \cdot 2H_2O$. (b) Shock adiabats for silicates: *1*, $LiAl[Si_2O_6]$; *2*, $Na[AlSiO_4]$; *3*, $MgSiO_3$; *4*, $K[AlSi_3O_8]$; *5*, $Be_3Al_2[Si_6O_{18}]$; *6*, $Ca_3[Si_3O_9]$; *7*, *8*, $Ca_2Mg_5[Si_4O_{11}]_2[OH]_2$; *9*, $CaFeSi_2O_6$; and *10*, $Al_2SiO_4[FOH]_2$. (c) Shock adiabats for basic and ultrabasic rocks: *1*, olivine diallagite; *2*, ore olivenite; *3*, olivenite-1; *4*, enstatite rock; *5*, olivenite-2; *6*, feldspatic peridotite; *7*, dunite-2; *8*, enstatite gabbro with olivine; *9*, dolerite (trapp); *10*, olivine diabase; and *11*, dunite-2.

of shock-wave parameters is detected. This zone was interpreted as the phase transition of these materials occurring in the liquid state. From the very beginning, the results of the experiments of [61] gave rise to doubts. But the results of measurements presented in this paper have not been verified. And only the smooth monotonic curve of wave-velocity decay obtained in underground nuclear explosions [67] served as an indicator of the incorrectness of measurements [61].

9. Rocks

The interest in studies of shock compression of rocks and the need for their realization had two main reasons:

(1) technical tasks associated with surface rock explosions;

(2) problems connected with the composition of the internal regions of the Earth's mantle.

The most complete work devoted to surface rock compression [68] generalizes the results of studies of more than 100 individual rocks of magmatic and sedimentary types. Their average values are shown in Fig. 17.

Qualitatively, the majority of adiabats of magmatic type represent similar dependences with close parameters, namely, a flat initial part (treated as a phase transition in rocks) and steep second part (compression of dense phases) with a slope varying (at $D = 11-12$ km s^{-1}) from $D'_U = 1.5-1.6$ to

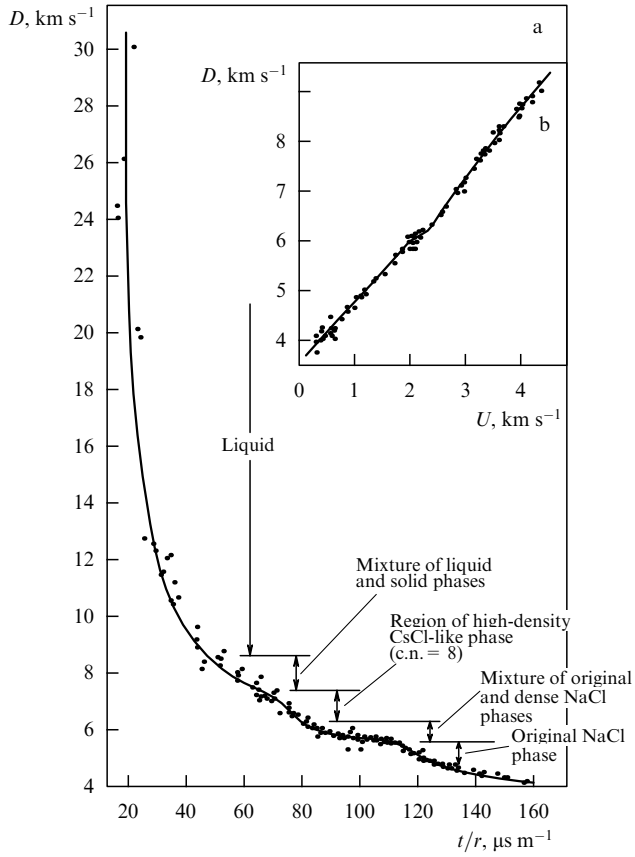

Figure 16. (a) Shock-wave decay as a function of the reduced distance during nuclear explosions in rock salt. Refined position in the phase transition region.

$D'_U = 1.2$. Note that in the dense-phase region the slopes of magmatic-type adiabats are similar both to each other and to the slopes of adiabats of quartz- and silica-type rocks. The first flat part of the adiabats of the magmatic rocks with a complex mineral composition and structure possibly reflects the 'averaged' (under the effect of pressure) properties of separate minerals. On the $D-U$ diagram, a single 'averaged' two-phase flat curve appears.

No such a similarity is observed for adiabats of sedimentary rocks. The compression curves for clay and calcite rocks are characterized by qualitatively different $D(U)$ dependences, except for shale and sandstone, whose adiabats are similar to those of magmatic rocks.

We should say a few words about the stability of shock adiabats for rocks with respect to variations of the thickness of the samples studied, i.e., to the scale variation of experiments. The results of laboratory tests (sample thickness of several millimeters) were compared with the measurements in underground nuclear explosions (sample thickness of the order of tens of centimeters) for two typical rocks: shale and dolomite. Coincident results were obtained for both rocks. This indicates (just as mentioned above for silica) the absence of the scale factor in shock compression of the rocks. Evidently, it would not be a great mistake to expand these conclusions to other rocks.

Paper [69] summarizes the results of studies of deep-seated rocks, mostly, of olivine and enstatite types. Essentially, it was the first and the only paper specially aimed at (in order to solve some geophysical problems) considering the compression of a great amount of ultrabasic and basic rocks up to a maximum pressure of 200 GPa (in some cases up to 500 GPa), which essentially (by more than an order of magnitude) exceeds the pressures reached by foreign scientists. The obtained adiabats (Fig. 15c) in the $D-U$ coordinates represent lines with similar slopes and are characterized by breaks in $D(U)$ dependences related to phase transformations. Data on the shock compression of olivine (Mg_2SiO_4) and enstatite ($MgSiO_3$) rocks were first used to estimate the content of these fractions in the Earth's mantle. The upper limits on the iron oxide content in the Earth's mantle near its border with the core were also derived in this paper from the comparison of experimental data on the shock compression of rocks with different iron content and the Earth model proposed by Bullen [70]. The mantle was shown to contain about 25% iron oxides. Unlike these estimates that can change depending on the chosen Earth model, the second conclusion on the iron-content change with the mantle depth seems to be valid for all models of the Earth's internal structure.

10. Calculated description of the rocks and minerals

As mentioned above, phase transitions occurring at certain pressures from the initial states to denser and strongly compressed phases are a common property of rocks and minerals. According to data of [71, 72], the phase transitions in these systems result in the formation of an isochemical mixture of close-packed oxides of metals and silicon. This fact was used in [38] to reproduce from oxide compositions the additive equations of state for minerals and rocks and to obtain the shock adiabats of the corresponding compounds. The experimental results and calculations (Fig. 18) were compared in [38] and the coincidence was found to be very good. However, in some cases the slopes of the calculated additive adiabats are greater than the slopes of experimental adiabats.

The rocks and minerals, have some common properties namely;

— adiabats are linear in the $D-U$ coordinates (over a certain interval of velocities),

— the slopes D'_U are relatively close for many rocks and minerals,

— phase transitions are observed in both.

These common properties were used in [73] to consider the problem of the correlation of the oxide composition with dynamic adiabats. For all rocks, minerals, and rock-forming oxides, a method of correlation-regression analysis of experimental data was applied to obtain the simplest analytic dependences

$$C = C_0(z, \rho_0)\,, \quad a = a(z, \rho_0)\,.$$

After testing the adequacy of the experimental data description by the linear equation

$$D = C_0(z, \rho_0) + a(z, \rho_0)U$$

these dependences can be used to calculate shock adiabats of rocks and minerals.

The functions for C_0 and a were chosen in the form of multiregression equations:

$$C_0 = a_0 + a\rho_0 + \sum a_i z_i\,, \quad a = b_0 + b\rho_0 + \sum b_i z_i\,.$$

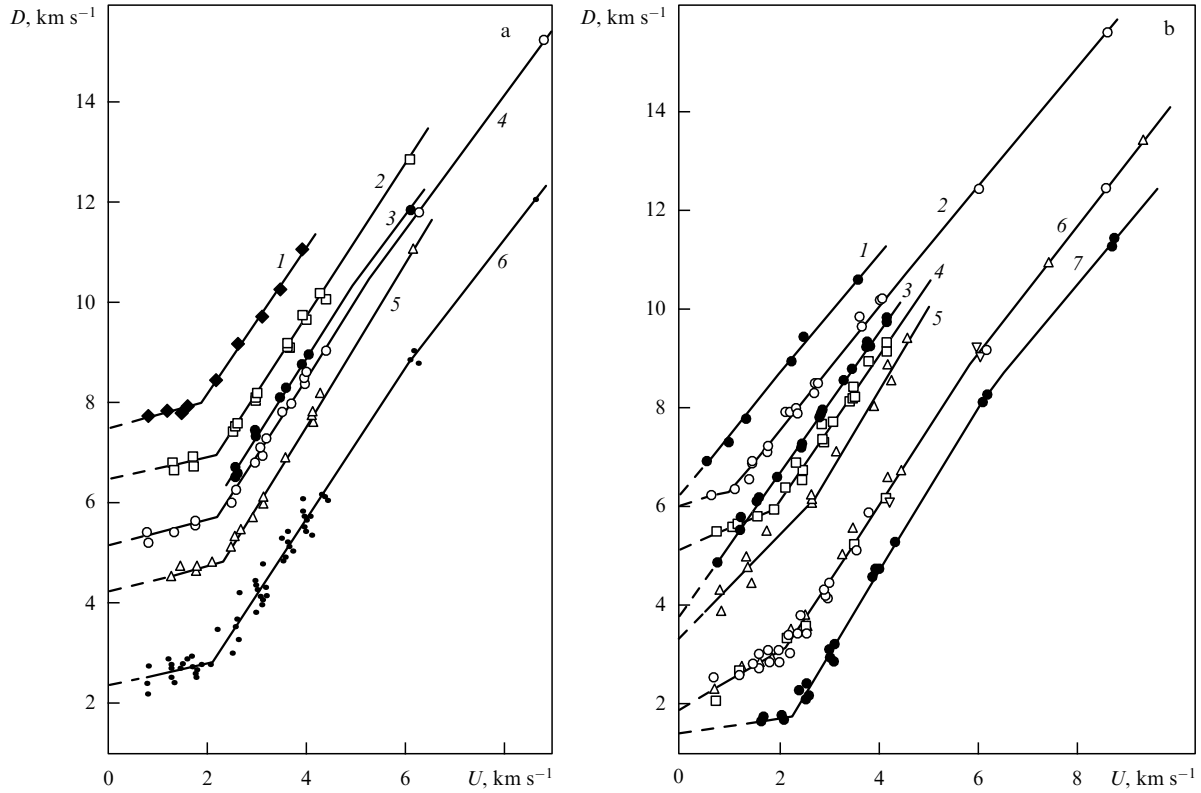

Figure 17. (a) $D-U$ diagram for magmatic rocks: *1*, gabbro ($D+2$); *3*, tuffs; *4*, granites; *5*, porphyries ($D-1$); *6*, average adiabat for magmatic rocks ($D-3$). (b) $D-U$ diagram for sedimentary rocks: *1*, magnesite; *2*, dolomites; *3*, limestone; *4*, aleurolites; *5*, clays; *6*, shale ($D-3$); and *7*, sandstone ($D-4$).

Here, z is the percentage of the corresponding components in the material; and a_0, a, a_i, b_0, b, and b_i are the coefficients in the equations. Numerical values of the coefficients can be found from the elemental composition of the compounds under consideration.

Figure 18 demonstrates a satisfactory agreement between calculations and experimental results for certain mineral adiabats. In our practical activity related to underground nuclear explosions, we always had to apply such estimates for rock adiabats.

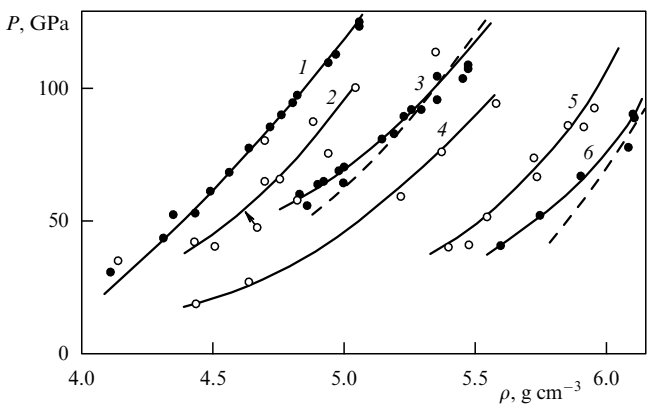

Figure 18. Calculated adiabats for minerals and rocks: *1*, MgO; *2*, SiO_2(2); *3*, enstatite rock ($\rho+2$); *4*, calcite ($\rho+1$); *5*, granite ($\rho+1$); and *6*, albitite ($\rho+1.3$). The dashed line, calculations [38]; the solid line, calculations [73].

11. Liquids

11.1 Water and its solid modifications

Being the most widespread liquid in the nature, water became the first liquid to be studied. The main problem to be solved with these experiments was the construction of the equation of state for water. This equation was necessary in various calculations of pulse loading effects on underwater and on-water constructions. Data on water compression have also been required in analysis of compounds containing water as one of the components.

The studies of shocked-water properties started in the 1950s [74, 75]. At that time, data for water compression were obtained up to a pressure of 20 GPa in the United States and up to 80 GPa in Russia. Later on, these results were elaborated in many papers [29, 77] and the limiting pressure was increased up to 3000 GPa [46].

At the end of 1970s, the first data on the compression of finely dispersed snow powder and ice (solid modifications of water) were published. The maximum pressure at which the ice is melted is a few gigapascals, so we can consider that dynamic adiabats for ice and snow at high pressures characterize the compressibility of the liquid phase irrespective of the initial state. In [78], these results were substantially extended by experiments with smaller initial densities. Some data from [29] were refined and supplemented with measurements at low pressures.

Figures 19a–19c illustrate joint results of laboratory experiments in the $D-U$, $P-\rho$, and $T-P$ coordinates. In the first figure, the adiabat for 'solid' water is compared

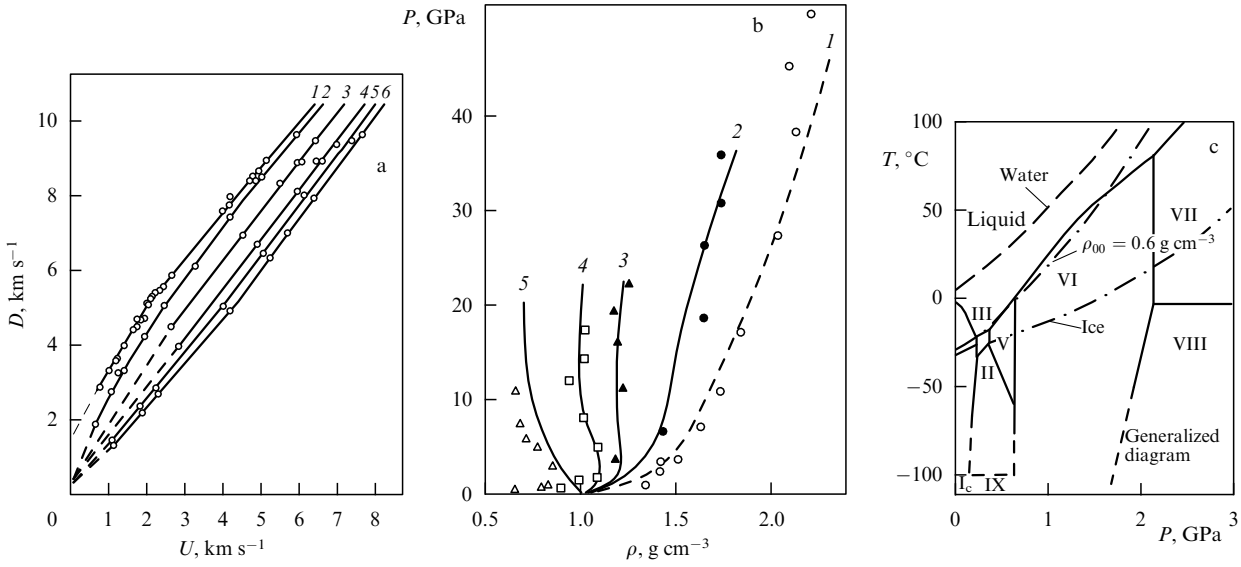

Figure 19. (a) $D-U$ diagram for water, ice, and snow: *1*, water; *2*, ice; *3*, snow with densities $\rho_{00} = 0.6$, 0.35, 0.25, and 0.15 g cm^{-3}, respectively. (b) $P-\rho$ diagram for water (solid lines, calculations [76]; dashed line, water adiabat): *1*, ice ($\rho_{00} = 0915$ g cm^{-3}); *2–5*, ice with $\rho_{00} = 0.6$, 0.35, 0.25, and 0.15 g cm^{-3}, respectively. (c) Phase diagram for water (solid lines, phase boundaries; dot-and-dash lines, shock adiabats).

with the corresponding porous adiabats. Note some features of them.

First, all the adiabats, including that for ice (the difference between the ice and water density is less than 10%), center around one point $D_0 = 0.15$ km s^{-1} (or of small neighborhood of it). This is similar to the previously considered behavior of porous metals, for which $D_0 \approx$ const are qualitatively explained by their correspondence to the sound velocity in air reduced by metal particles inside the samples.

The second peculiarity (common with metals) is associated with changes in the adiabat slope D'_U. At $U < 3$ km s^{-1}, they differ by more than two times. But with increasing D and U, the slopes of the adiabats already get closer in the experimentally studied region and approach the limit $D'_U = 1.2-1.3$ in the high-pressure region. The reason for this change is still unknown. Perhaps, this relates to the loss of the short-range atomic order in the 'crystal' lattice of water and its solid modifications and, therefore, to the transition to disordered atomic structure. To answer this question, more precise methods than we used are required.

Finally, the position of the lower seven–eight points of the ice adiabat in the $P-\rho$ diagram is very interesting (Fig. 19b). These points lie (in compressibility) to the right of water points. This cannot be explained by the 'measurement errors': to 'shift' these point to the left of the water adiabat, the shock wave velocity should be increased by $\Delta D \geqslant 200$ m s^{-1}. Such an error is excluded due to the large number of experimental points. Assumptions like the 'nonequilibrium' of the detected states are hardly reasonable as well. This fact could be explained by water–ice phase transitions. Indeed, let us compare the states on porous and solid water adiabats on the $P-T$ diagram with the water phase diagram. Figure 19c shows the initial part of this diagram [79]. Shock adiabats for water, ice, and porous ice with $\rho_{00} = 0.6$ g cm^{-3} are also plotted. The temperature on the shock adiabats is evaluated using the equation of state from [29].

We conclude that on the $P-\rho$ diagram of the ice, the shock adiabat is located in the region of solid modifications of water — ices *III*, *V*, *VI*, and *VII*. Due to high porosity and, hence, high heating, all adiabats but one are in the region of liquid. An exception is the adiabat with $\rho_{00} = 0.6$ g cm^{-3}, which possibly 'goes' into the region of solid states for pressures $\leqslant 2$ GPa. The water adiabat also lies in the liquid region, where water states are characterized by higher temperatures than ice states.

Let us return to the $P-\rho$ diagram. For porosity $m > 2.86$, the slope $(\mathrm{d}P/\mathrm{d}\rho)_{\mathrm{H}}$ of experimental adiabats alters the sign from positive at small pressures ($P < 5$ GPa) to negative for the maximum experimental pressure. Alternating adiabats of compounds were obtained in these studies for the first time.

Such were the brief conclusions from the analysis of the shock adiabats for water and porous ice.

11.2 Compression of water solutions

Now consider the shock compression of saturated water solutions of several salts. The saline solutions of eight halogenides, two sulfates, and one thiosulfate were studied in [80]. The data obtained are compared with the water adiabat in Fig. 20a. It is seen that the experimental points for solutions lie near the water shock adiabat and generally repeat its peculiarities: a broken line with a steep first segment ($D'_U = 1.8$) and a relatively flat second part ($D'_U = 1.2-1.3$)). The transition from the first to the second part for solutions is similar to the corresponding transition for water and occurs at $D \approx 4-5$ km s^{-1}. Note that the adiabats of solutions are away from the water adiabat by the amount ΔD, which is the difference between the sound velocity in water ($C_0 \approx 1.5$ km s^{-1}) and in the corresponding solution. This may imply that the adiabats of the saline solutions with lower concentrations will lie between those of water and the saturated solution of the corresponding saline.

The similarity of the shock adiabats of different saline solutions allows one to admit that the $D(U)$ dependences of aqueous solutions of other salts will also be similar to the water adiabat. The new type of compound that represents a homogeneous two-component system located amid the chemical compounds and mechanical mixtures, in the first approximation, corresponds to the specific-volume additivity

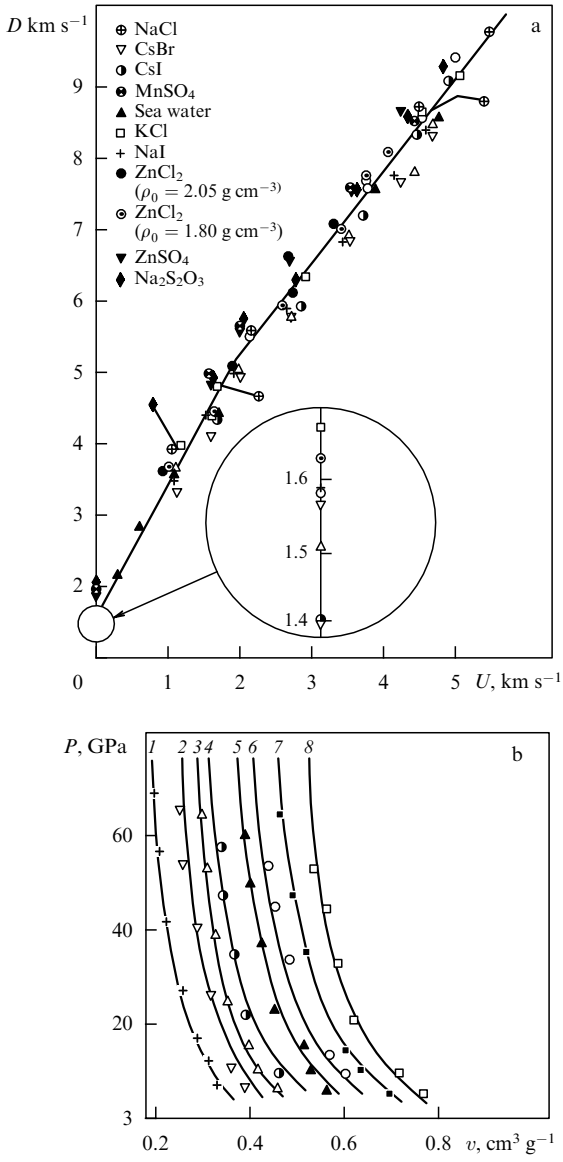

Figure 20. (a) $D-U$ diagram for saturated solutions of various salts (the solid line is the water adiabate). (b) Comparison of the results of experiments with additive calculations: *1*, NaI ($v-0.05$ g cm^{-3}); *2*, CsBr; *3*, KI ($v+0.03$ g cm^{-3}); *4*, CsI; *5*, $Na_2S_2O_3$ ($v+0.04$ g cm^{-3}); *6*, KBr ($v+0.05$ g cm^{-3}); *7*, NaCl ($v+0.1$ g cm^{-3}); and *8*, KCl ($v+0.15$ g cm^{-3}).

rule, directly applied to shock adiabats of the initial materials [80]. In these estimates, the shock adiabats of water and of the corresponding salines were taken as the initial ones. Figure 20b compares the calculations with experiments. The accordance appears to be satisfactory, i.e., the additivity principle is valid for dynamic adiabats of all presented saturated solutions. It seems that this conclusion can be applied to the lower concentrated solutions of the studied compounds too.

12. Compression of organics

In the last decade, this class of materials has been extensively applied in different scientific and engineering systems, including those operating under heavy pulse loadings. This calls for investigation of their thermodynamic properties in the domain of high pressures and temperatures.

However, it is clear that the direct study of properties of organics is impossible in practice due to their unlimited number. So, the first problem was to propose a model to calculate (estimate) their properties, the shock adiabats first of all. But any model should be tested by experimental data. Therefore, primarily the task was reduced to collecting and accumulating concrete experimental results. To this end, all organic compounds were divided into a few large groups:

1. *Saturated hydrocarbons* (*alcanes*) C_nH_{2n+2}. Data on compression of these materials are collected in [81].
2. *Unsaturated hydrocarbons* (*alkenes* C_nH_{2n} and *alkynes* C_nH_{2n-2} [82]).
3. *Aromatic hydrocarbons* (hydrocarbons with benzene base $C_6H_{5+\alpha}$) [81].
4. *Alcohols* $C_nH_{2n+1}OH$ [82].
5. *Monobasic acids* $C_nH_{2n+1}COOH$ [82].
6. *Anhydrides* $(C_nH_{2n+1}CO)_2O$ [82, 83].
7. *Ketones*. Two compositions of this class are acetone $(CH_3)_2CO$ and cyclohexanone ($C_6H_{10}O$) [82].
8. *Solid organic materials* — polyethylene, plexiglass, etc. [83]

The results of shock compression studies of organics were published in the above-cited papers. Here, we present the main conclusions derived from analysis of the experimental data. They can be summarized as follows. There are two types of shock adiabats of organics. The first type is characterized by a mass-velocity jump with $D \approx$ const. In the $P-\rho$ diagram, this corresponds to a density jump with weakly changing pressure. The second type are 'broken' adiabats; they can be represented by two crossing straight lines with different slopes in the $D-U$ coordinates and by two parabolic curves conjugated at the crossing point in the $P-\rho$ coordinates. This form of adiabat indicates significant structure transformations in shocked organics.

These transformations can be assumed to result from the rupture of covalent bonds between C and H atoms and the formation of new C-C diamond bonds and H – H molecular hydrogen bonds (similar for nitrogen and oxygen). Other assumptions about the final decomposition products are quite possible. For example, Voskoboinikov [85] suggested a composition with condensed methane as the main component. However, from our point of view, the assumption on the simplest elemental form of the final composition is more attractive. This is indirectly indicated by suitable agreement between the volumes of hydrocarbons extrapolated to $P=0$ in the high-density branches and the additive volumes of diamond and molecular hydrogen (for the corresponding materials). The difference between additive volumes (at $P=0$) V_{add} and those obtained from the linear extrapolation of the upper parts of adiabats (associated with high-density phases) does not exceed 2% as a rule. Such a coincidence cannot be chance.

Note the results of multistage shock compression experiments with some organic liquids placed in special 'safety ampules.' Maximum pressures were about 40 GPa. After the shock wave passage, an amorphous soot powder remained in the preserved ampules (it proved impossible to retain hydrogen in incompletely hermetic ampules). The important experimental result of relevance here was the decomposition of the initial structures to elementary components.

Thus, there is indirect evidence of the decomposition reactions occurring in C – H compounds.

To investigate the possibility of the construction of high-density parts of hydrocarbon shock adiabats using an additive mixture of the components, an attempt was made to simply add the specific volumes of hydrogen and diamond

(according to their fractions in the mixture) along the shock adiabats. The results were unsuccessful. So, as in [84], the equation of state in the Mie – Grüneisen form was taken to obtain the additive adiabats:

$$P(V,T) = P(V,0) + \frac{\gamma}{V}\left[E(V,T) - E(V,0)\right].$$

Here, $P(V,0)$ and $E(V,0)$ are the cold ($T = 0$ K) components of pressure and energy, $P(V,T)$ and $E(V,T)$ are the warm components, γ is the Grüneisen coefficient, and V is the specific volume. For cold isotherms, the following expression is adopted:

$$V(P,0) = XV^{\mathrm{C}}(P,0) + (1-X)V^{\mathrm{H}}(P,0),$$

which is valid for chemically inert atoms of hydrogen and carbon. For γ, the relation

$$\frac{V}{\gamma} = X\left(\frac{V}{\gamma}\right)^{\mathrm{C}} + (1-X)\left(\frac{V}{\gamma}\right)^{\mathrm{H}}.$$

is assumed.

In these dependences, X is the weight fraction of carbon, the indices C and H correspond to carbon (diamond) and hydrogen, respectively. As in [84], $(V/\gamma)^{\mathrm{C,H}}$ are assumed to be constant and independent of V and T (their values were taken from [84]): for diamond, $V/\gamma = 0.335$ cm^3; for hydrogen 3.0 cm^3.

Materials with smooth shock adiabats [smooth $D(U)$ functions] centered at V_0 (the initial, 'experimental' specific volume) are presented in the form

$$P_{\mathrm{H}} = \left[P(V,0) + \frac{\gamma}{V}\int_{V_0}^{V} P(V,0)\,\mathrm{d}V\right]\left[1 - \frac{\gamma}{2V}(V_0 - V)\right]^{-1}$$

(adiabats of diamond and molecular hydrogen are of this type).

Adiabats of organic compounds that consist of a hydrogen – diamond 'mixture' at high pressures are characterized (in $P-V$ coordinates) by two segments: the first one centered at the initial volume V_{00} (at $P = 0$), and the second 'mixed' region corresponding to the extrapolated value V_0' (the initial mixed phase volume). The adiabat of the dense phase can be written in the form

$$P_{\mathrm{H}}' = \left\{P_{\mathrm{H}}\left[1 - \frac{\gamma}{2}\left(\frac{V_0}{V} - 1\right)\right] + \frac{\gamma}{V}[E_0' - E_0]\right\} \times \left[1 - \frac{\gamma}{2}\left(\frac{V_0'}{V} - 1\right)\right]^{-1}.$$

Here, E_0' is the initial energy. The effect of reasonable variations of $E_0' - E_0$ on P_{H}' is small and can be neglected. From the known shock adiabats of diamond, hydrogen, oxygen, and nitrogen, their cold compression curves can be derived. Using known values of V/γ from [84], the adiabat compression parameters P_{H}' of various materials can be obtained (see [81 – 83], among others).

In Figure 21 we compare calculated and experimental data for some organics of both types ('broken' and 'discontinuous' adiabats). The coincidence between experimental results and calculations justifies the assumption about the disruption of molecular bonds C – H (C – H – N – O) with the formation of a two-phase mixture: carbon (diamond) and molecular hydrogen (or oxygen and nitrogen). The same coincidence takes place for other materials which we did not mention here.

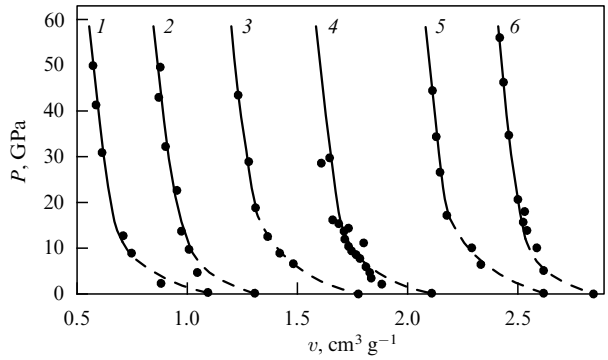

Figure 21. Additive calculations of shock adiabats for organic compounds: *1*, formic acid; *2*, tetracosane; *3*, cyclohexanone ($v + 1$); *4*, nitrobenzene ($v + 3$); *5*, octyl alcohol ($v + 2$); and *6*, plexiglass ($v + 2$).

This model was checked for more than 30 different materials and seems to be applicable to other hydrocarbon compounds. Here, we should note that its applicability is limited by pressures $P > 20$ GPa. At these pressures, 'reconstructions' of shock adiabats complete.

13. Conclusion

In our review, we presented the generalized results of laboratory measurements of shock compression for a broad range of materials, from elements and their alloys to complex compounds. These studies are of interest both for physics of high energy densities and for numerous technical applications. The data considered can be used as a basis for constructing equations of state for various materials.

Based on the experimental data analysis, the following main results have been obtained.

— Shock adiabats for elements are classified by the type of $D(U)$ dependences. Over broad range of kinematic parameters, shock adiabats for elements are shown to 'approach' a limiting regime with a slope $D_U' = 1.2 - 1.3$.

— For materials with a large degree of porosity ($m > 20$), the adiabats in the $D-U$ plane are located immediately close to the limiting dependence $D = U$. This implies that measurements for $m > 20 - 30$ become worthless, since in these coordinates new data will be quite similar to already obtained 'limiting' adiabats.

— A qualitative similarity is found in the adiabat location for porous elements and various compounds. This implies the existence of a common value D_0 at $U = 0$ (or a small interval ΔD_0) for all materials and for all degrees of porosity m. This also suggests the transition of all adiabats (with increase of kinematic parameters) to $D(U)$ dependences, characterized by the same critical slope $D_U' = 1.2 - 1.3$.

— From comparison of adiabats of metals referring in the initial states to two different phases, solid and liquid (preliminarily melted samples), a conclusion is made about the sample melting on the shock adiabat of the 'cold' metal at the parameters at which the functions D and U and their derivatives coincide for both adiabats.

— The peculiarities of adiabats of different compounds were found. Using these properties, it became possible in the framework of additive solutions to estimate the location of adiabats of materials of the same types as the studied ones.

In addition to reviewing the strong shock compression of materials in underground nuclear explosions [3], the present paper concludes some studies in this field.

To conclude, I am much obliged to the scientists from the All-Russia Research Institute of Experimental Physics, who provided the main contribution to the shock compression studies of different materials. The author was happy to collaborate with an outstanding collective of adherents. These were unforgettable years when the only motivation of our research was the wish to do as much as possible for the scientific prestige and the defense of our country, when we were not pressed by financial problems and limitations, and when personally for us the results were the only unselfish interest of our job.

The main contribution in these studies was made by the oldest researchers of the institute, with most of whom the author has worked for decades. These are:

L V Al'tshuler — the founder of the dynamic branch of studies of material properties. With his leadership and participation, fundamental results on the shock compression of metals were obtained. He contributed a lot to make me as a physicist.

A A Bakanova — my first mentor, with whom we made numerous joint studies on the shock-compressed metal properties. She acquainted me with experiments.

V N Zubarev — an acute researcher. He profoundly comprehended the essence of the studied phenomena and generously shared his knowledge with colleagues and comrades.

G V Simakov — my nearest colleague and co-author of most papers. He passed a 40-year part of research with me.

M N Pavlovskiĭ — who laid the foundation to the construction of the plane-wave measurement systems widely used in our research. He performed an extensive study on shock compression of many (in particular ultrahard) materials.

M A Podurets, whose penetrating theoretical understanding of the processes studied, his sincere interest in the results of experiments and his initiative in setting some tests strongly promoted the success of their performance.

M V Zhernokletov and G S Telegin, with whom I carried out the studies on compression of organics, rocks, and some other materials.

And finally, V A Bugaeva, V V Dorokhin, I P Dudoladov, A A Evstigneev, N F Kuznetsov, B N Moiseev, L V Popov, Yu N Sutulov, V V Shutov, and many other researchers who directly took part in the studies of the shock compression of materials.

There have been many others colleagues not mentioned here, who during all these years sincerely devoted themselves, their experience and knowledge to our science, high-energy-density physics. Even the simple enumeration of their names would take too much place in this paper. That is why I have to restrict myself by only saying words of sincere gratitude to them for their unselfish and essentially unpaid labor.

I am grateful to B L Glushak, who kindly acquainted with the draft of this review and made some useful remarks on the essence of the paper, and to N L Shaboldina, who assisted me in the manuscript preparation.

References

1. Al'tshuler L V et al. *Usp. Fiz. Nauk* **166** 575 (1996) [*Phys. Usp.* **39** 539 (1996)]
2. Al'tshuler L V, Krupnikov K K, Brazhnik M I *Zh. Eksp. Teor. Fiz.* **34** 886 (1958) [*Sov. Phys. JETP* **7** 614 (1958)]
3. Trunin R F *Usp. Fiz. Nauk* **164** 1215 (1994) [*Phys. Usp.* **37** 1123 (1994)]
4. Al'tshuler L V et al. *Zh. Eksp. Teor. Fiz.* **34** 874 (1958) [*Sov. Phys. JETP* **7** 606 (1958)]
5. Bugaeva V A, Evstigneev A A, Trunin R F *Teplofiz. Vys. Temp.* **34** 684 (1996) [*High Temp.* **34** 674 (1996)]
6. Dandekar D P *J. Appl. Phys.* **47** 4703 (1976)
7. Dremin A N, Kanel' G I *Zh. Prikl. Mekh. Tekh. Fiz.* (2) 146 (1976)
8. Podurets M A et al. *Izv. AN SSSR. Ser. Fiz. Zemli* (6) 26 (1989)
9. Al'tshuler L V et al. *Fiz. Tverd. Tela* **5** (1) 279 (1963)
10. Al'tshuler L V et al. *Zh. Eksp. Teor. Fiz.* **38** 790 (1960) [*Sov. Phys. JETP* **11** 573 (1960)]
11. Al'tshuler L V, Bakanova A A, Trunin R F *Zh. Eksp. Teor. Fiz.* **42** 91 (1962) [*Sov. Phys. JETP* **15** 65 (1962)]
12. Al'tshuler L V et al. *Zh. Prikl. Mekh. Tekh. Fiz.* **22** (2) 3 (1981) [*J. Appl. Mech. Tech. Phys.* **22** 145 (1981)]
13. Trunin R F *Shock Compression of Condensed Materials* (Cambridge: Univ. Press, 1998)
14. Barker L M *J. Appl. Phys.* **46** 2544 (1975)
15. Al'tshuler L V, Bakanova A A, Dudoladov I P *Pis'ma Zh. Eksp. Teor. Fiz.* **3** 483 (1966) [*JETP Lett.* **3** 315 (1966)]
16. Al'tshuler L V, Bakanova A A *Usp. Fiz. Nauk* **96** 193 (1968) [*Sov. Phys. Usp.* **11** 678 (1969)]
17. Carter W J et al. *J. Phys. Chem. Solids* **36** 741 (1975)
18. Trunin R F et al. *Teplofiz. Vys. Temp.* **33** 222 (1995)
19. *Lasl Shock Hugoniott Data* (Los Alamos Series on Dynamic Material Properties, Ed. S P Marsh) (Berkeley: Univ. California Press, 1980)
20. Medvedev A B *Vopr. At. Nauki Tekh.* (1) 12 (1992)
21. Krupnikov K K, Brazhnik M I, Krupnikova V P *Zh. Eksp. Teor. Fiz.* **42** 675 (1962) [*Sov. Phys. JETP* **15** 470 (1962)]
22. Kormer S B et al. *Zh. Eksp. Teor. Fiz.* **42** 686 (1962) [*Sov. Phys. JETP* **15** 477 (1962)]
23. Trunin R F, Simakov G V *Zh. Eksp. Teor. Fiz.* **103** 2180 (1993) [*JETP* **76** 1090 (1993)]
24. Trunin R F et al. *Zh. Eksp. Teor. Fiz.* **96** 1024 (1989) [*Sov. Phys. JETP* **69** 580 (1989)]
25. Simakov G V, Trunin R F *Izv. Akad. Nauk SSSR Ser. Fiz. Zemli* (11) 72 (1990) [*Izv. Acad. Sci. USSR. Phys. Solid Earth* **26** 952 (1990)]
26. Ragan Ch. III *Phys. Rev. A* **29** 1391 (1984)
27. Zubarev V N et al., in *Dokl. I Vsesoyuzn. Simp. po Impul'snym Davleniyam* (I All-Unit Symp. on Pulsed Pressures) Vol. 1 (Moscow: VNIIFTRI, 1974) p. 61
28. Podurets M A et al. *Izv. Akad. Nauk SSSR Ser. Fiz. Zemli* (1) 16 (1981)
29. Bakanova A A et al. *Zh. Eksp. Teor. Fiz.* **68** 1099 (1975) [*Sov. Phys. JETP* **41** 544 (1975)]
30. Trunin R F, Simakov G V, Medvedev A B *Teplofiz. Vys. Temp.* **37** 732 (1999) [*High Temp.* **37** 851 (1999)]
31. Urlin V D *Zh. Eksp. Teor. Fiz.* **49** 485 (1965) [*Sov. Phys. JETP* **22** 341 (1966)]
32. Sapozhnikov A T, Pershina A V *Vopr. At. Nauki Tekh.* (4) 47 (1975)
33. Glushak B L et al. *Vopr. At. Nauki Tekh.* (2) 57 (1991)
34. Al'tshuler L V, Brusnikin S E *Teplofiz. Vys. Temp.* **27** (1) 42 (1989) [*High Temp.* **27** 39 (1989)]
35. Bakanova A A, Dudoladov I P, Sutulov Yu N *Zh. Prikl. Mekh. Tekh. Fiz.* (6) 167 (1972)
36. Belyakova M Yu et al. *Izv. Akad. Nauk SSSR Ser. Fiz. Zemli* (1) 99 (1991) [*Izv. Acad. Sci. USSR. Phys. Solid Earth* **27** 71 (1991)]
37. Bakanova A A et al. *Izv. Ross. Akad. Nauk. Ser. Fiz. Zemli* (6) 58 (1995)
38. Al'tshuler L V, Sharipdzhanov I I *Izv. Akad. Nauk SSSR Ser. Fiz. Zemli* (3) 11 (1971)
39. Pavlovskiĭ M N *Fiz. Tverd. Tela* **13** 893 (1971)
40. Larin B N *Gipoteza Iznachal'no Gidridhoĭ Zemli* (Hypothesis of an Initially Hydride Earth) 2nd ed. (Moscow: Nedra, 1980)
41. Trunin R F et al. *Izv. Akad. Nauk SSSR Ser. Fiz. Zemli* (11) 65 (1987) [*Izv. Acad. Sci. USSR. Phys. Solid Earth* **23** 919 (1987)]
42. Adadurov G A et al. *Zh. Prikl. Mekh. Tekh. Fiz.* (4) 81 (1962)
43. Wackerle J *J. Appl. Phys.* **33** 922 (1962)

44. Al'tshuler L V, Trunin R F, Simakov G V *Izv Akad. Nauk SSSR. Ser. Fiz. Zemli* (10) 1 (1965)
45. Trunin R F et al. *Izv. Akad. Nauk SSSR Ser. Fiz. Zemli* (1) 13 (1971)
46. Avrorin E N et al. *Pis'ma Zh. Eksp. Teor. Fiz.* **31** 727 (1980) [*JETP Lett.* **31** 685 (1980)]
47. Trunin R F, Simakov G V, Podurets M A *Izv. Akad. Nauk SSSR. Ser. Fiz. Zemli* (2) 33 (1971)
48. Podurets M A et al. *Izv. Akad. Nauk SSSR Ser. Fiz. Zemli* (11) 59 (1976)
49. Simakov G V, Trunin R F *Izv. Akad. Nauk SSSR Ser. Fiz. Zemli* (2) 72 (1990)
50. Vildanov V G et al., in *Shock Compression of Condensed Matter – 1995* Vol. 1 (Eds S C Schmidt, W C Tao) (New York: American Institute of Physics, 1995) p. 121
51. Holmts N C, Sce E F, in *Shock Compression of Condensed Matter – 1991* (Eds S C Schmidt, R D Dion) (Amsterdam: North-Holland, 1992) p. 91
52. Podurets M A, Simakov G V, Trunin R F *Izv. Akad. Nauk SSSR. Ser. Fiz. Zemli* (7) 3 (1976)
53. Podurets M A, Simakov G V, Trunin R F *Izv. Akad. Nauk SSSR. Ser. Fiz. Zemli* (4) 30 (1990) [*Izv. Acad. Sci. USSR. Phys. Solid Earth* **26** 295 (1990)]
54. Furuish M D, Ito E J, in *Proc. 1995 ARC Topical Conference on Chock Compression of Condensed Matter* (Seattle, WA, 1995)
55. Al'tshuler L V et al. *Fiz. Tverd. Tela* **15** 1436 (1973)
56. Simakov G V, Podurets M A, Trunin R F *Dokl. Akad. Nauk SSSR* **211** 1330 (1973)
57. Kalashnikov N G et al. *Izv. Akad. Nauk SSSR Ser. Fiz. Zemli* (2) 23 (1973)
58. Simakov G V et al. *Izv. Akad. Nauk SSSR Ser. Fiz. Zemli* (8) 11 (1974)
59. Simakov G V, Trunin R F *Izv. Akad. Nauk SSSR Ser. Fiz. Zemli* (2) 77 (1980)
60. Al'tshuler L V et al. *Fiz. Tverd. Tela* **5** 279 (1963)
61. Kormer S B et al. *Zh. Eksp. Teor. Fiz.* **47** 1202 (1964) [*Sov. Phys. JETP* **20** 811 (1965)]
62. Liu L, Bassett W A *J. Appl. Phys.* **44** 1475 (1973)
63. Piermarini G J, Block S *Rev. Sci. Instrum.* **46** 973 (1975)
64. Al'tshuler L V, Kuleshova L V, Pavlovskiĭ M N *Zh. Eksp. Teor. Fiz.* **39** 16 (1960) [*Sov. Phys. JETP* **12** 10 (1961)]
65. Kuleshova L V, Pavlovskiĭ M N *Fiz. Tverd. Tela* **18** 573 (1976)
66. Alder B , in *Solids under Pressure* (Eds W Paul, D M Warschauer) (New York: McGraw-Hill, 1963) [Translated into Russian (Moscow: Mir, 1966) p. 430]
67. Podurets M A et al. *Fiz. Tverd. Tela* **34** 864 (1996)
68. Trunin R F et al. *Izv. Akad. Nauk SSSR Ser. Fiz. Zemli* (1) 52 (1988) [*Izv. Acad. Sci. USSR. Phys. Solid Earth* **24** 38 (1988)]
69. Trunin R F et al. *Izv. Akad. Nauk SSSR Ser. Fiz. Zemli* (9) 1 (1965)
70. Bullen K E *Seismology* (London: Methuen, New York: Wiley, 1954) [Translated into Russian: *Seĭsmologiya i Vnutrennee Stroenie Zemli v Tselom* (Moscow: IL, 1958)]
71. Birch F *J. Geophys. Res.* **57** 227 (1952)
72. Ringwood A E *Phys. Earth Planet. Inter.* **3** 109 (1970)
73. Telegin G S et al. *Izv. Akad. Nauk SSSR Ser. Fiz. Zemli* (5) 22 (1980)
74. Walsh J M, Rice M H *J. Chem. Phys.* **26** 815 (1957)
75. Al'tshuler L V, Bakanova A A, Trunin R F *Dokl. Akad. Nauk SSSR* **121** (1) 67 (1958)
76. Podurets M A et al. *Zh. Eksp. Teor. Fiz.* **62** 710 (1972) [*Sov. Phys. JETP* **35** 375 (1972)]
77. Volkov L P et al. *Pis'ma v Zh. Eksp. Teor. Fiz.* **31** 546 (1980) [*JETP Lett.* **31** 513 (1980)]
78. Trunin R F et al. *Teplofiz. Vys. Temp.* **37** 732 (1999) [*High Temp.* **37** 702 (1999)]
79. Tonkov E Yu *Fazovye Prevrashcheniya Soedineniĭ pri Vysokom Davleniĭ* . Handbook (Phase Transformations of Compounds at High Pressures) (Moscow: Metallurgiya, 1988) p. 29
80. Trunin R F et al. *Izv. Akad. Nauk SSSR Ser. Fiz. Zemli* (12) 37 (1987)
81. Trunin R F et al *Khim. Fizika* **8** 539 (1989)
82. Trunin R F et al. *Khim. Fizika* **11** 424 (1992)
83. Trunin R F et al. *Khim. Fizika* **11** 557 (1992)
84. Ree F H *J. Chem. Phys.* **70** 974 (1979)
85. Voskoboinikov I M *Khim. Fizika* **5** 697 (1986)